Exploring Thermoelectric Effect Based on Multi-layer Conductor/Organic/Conductor Devices

A Dissertation Presented for the

Doctor of Philosophy

Degree

The University of Tennessee, Knoxville

Qing Liu

August 2016

Dedication

I dedicate my work to my parents!

Acknowledgements

I am sincerely thankful to my advisor Dr. Bin Hu for his five years of guidance and support for my research work and dissertation for my PhD degree. I learned a lot from him, most importantly the capability of deeply understanding research topic, solving problems and writing research papers. I am sure it may not be possible for me to finish my dissertation without his help. I would also thank the committee members for my dissertation defense, Dr. Roberto S. Benson, Dr. David J. Keffer, Dr. Zhanhu Guo for their instructive advice and great support.

I would be earnestly grateful to my collaborators for their great help in providing facilities and/or materials. They are Dr. Soo Young Park & Miss Haerim Nam from Seoul National University; Dr. David Mandrus & Dr. Rupam Mukherjee in University of Tennessee. I also would like to thank Dr. Lei Liu at University of Tennessee for the fruitful discussions.

I would like to show my gratitude to my former group members, Dr. Liang Yan, Dr. Wei Qin, Dr. Dehua Hu, Dr. Hongfeng Wang, undergraduate student Michael Stanford, Dr. Lei He, Dr. Huidong Zang, Dr. Ming Shao, Dr. Yue Wu, Dr. Zhihua Xu, Miss Lili Wu, & visiting scholar Jianping Xu for their great help in many valuable discussions. I also owe sincere and heartiest thankfulness to my current group members, Mingxing Li, Yu-Che Hsiao, Dr. Mahshid Ahmadi, Dr. Shengbo Ma, Jeremy Tisdale, Miss Ting Wu, Hengxing Xu, Miaosheng Wang, & undergraduate student Gavin Hunt Dorrity for their numerous discussions and great help.

I would also like to thank my several years' roommates, the graduate students, Chunli Zhang, Yuanyuan Liu, Yan Zhang for their help and care in my everyday life.

Finally, I must express my great appreciation to my parents, my younger sister & my brother-in-law & my little nephew, and my boyfriend (husband now) for the support. Thank you all.

Abstract

Thermoelectric phenomena involve the simultaneous presence of both electrical and thermal currents. The entropy has been heavily used as the driving force to diffuse charge carriers between high and low temperature surfaces towards the development of Seebeck effects in thermoelectric devices. However, this driving force from entropy difference can cause an inverse relationship between Seebeck coefficient and electrical conductivity in the thermoelectric developments. Increasing the charge density can decrease the entropy difference to diffuse the charge carriers at a given temperature difference and lead to a decrease on the Seebeck coefficient developed by the entropy difference. Therefore, it is necessary to develop an additional driving in thermoelectric devices for development of Seebeck effect. In this dissertation, Chapter 1 presents an introduction to the concepts of thermoelectric effect, the widely-utilized organic materials in thermoelectric devices, and the peer publication review in order to cover the academic progress in this field. Meanwhile, the fundamental issues towards developing Seebeck effect is also discussed in this chapter. Chapter 2 studies the additional driving force of surface polarization to enhance Seebeck effect in vertical multi-layer metal/polymer/metal thin-film devices. Chapter 3 explores tunable Seebeck regimes between entropy and polarization differences based on vertical multi-layer electrode/organic/electrode thin-film devices. Chapter 4 studies conflicting problems in developing dual Seebeck and cooling effects in vertical organic thin-film devices by considering about the surface polarization effect from charge-phonon coupling. Chapter 5 focuses on using Seebeck effects to study n and p-type properties in organo-metal halide perovskites. Finally, Chapter 6 gives a short conclusion for the entire dissertation.

Table of Contents

List of Tables

List of Figures

Chapter 1

1 Introduction

1.1 History of thermoelectric study

The direct energy conversion between heat and electricity based on thermoelectric effects has drawn much attention in power generation and heat pumping. The efficiency of the thermoelectric energy conversion is an increasing function of the materials' non dimensional figure of merit (ZT).[1,2] The thermoelectric figure of merit ZT is defined by the relationship $ZT=(S^2\sigma/\kappa)T$, where S is the Seebeck coefficient, σ is the electrical conductivity, κ is the thermal conductivity, and $S^2\sigma$ is power factor. As shown in **Figure 1.1**, a Seebeck voltage (ΔV) can be measured between two ends of the sample under a temperature difference (ΔT), and the Seebeck coefficient is defined as S=ΔV/ΔT. By combining the n- and p-type legs in series, the Seebeck voltage would be enlarged by addition ($\Delta V=\Delta V_n+\Delta V_p$) for thermoelectric power generation.

Obtaining a figure of merit larger than one is important for thermoelectric power generation efficiency. Inorganic thermoelectric materials based on elements like Bi, Te, Sb, Pb, *etc*. can achieve *ZT* of unity at low temperatures (300–700 K).[3,4] In these materials, the carrier concentration can be modulated to generate a high electrical conductivity, while, the thermal conductivity always includes both electrical contribution (electrical carriers) and phonon contribution (lattice vibration) as the heat carriers. So thermal conductivity and electrical conductivity always couple with each other due to the electrical carriers. Reducing thermal conductivity without sacrificing electrical conductivity has been one of the major methods to enhance *ZT* values of inorganic thermoelectric materials. As to the thermal conductivity, the electrical contribution can be determined by carrier concentration and charge mobility, and the phonon contribution is determined by composing elements, lattice structures, various microstructure interface, *ect.*. Actually, bulk nanocomposites have been studied extensively, which are designed to restrict thermal conduction through phonon scattering at interface but not destroying electrical conductivities due to the increased carrier concentration.[3-5] Therefore, *ZT* values above one are well obtained in bulk nanocomposites of inorganic thermoelectric materials. However, the composing elements such as Bi, Te, Sb and Pb are toxic and not abundant, and the processing of inorganic materials is difficult, so the commercialization and wide application of

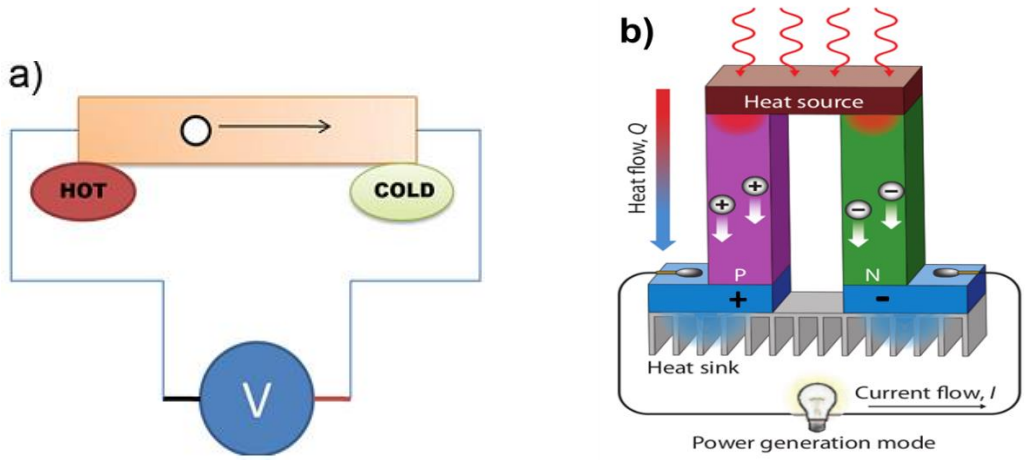

Figure 1.1 (a) A typical set-up for measurement of Seebeck coefficients ($S=\Delta V/\Delta T$);[6] (b) Schematic of thermoelectric power generation by a pair of p- and n- type legs in series.

inorganic thermoelectric materials are limited. On the other hand, organic thermoelectric materials are becoming more and more attractive because organic materials possess good flexibility and solution-processability and they are low-cost. In particular, thermal conductivity of organic materials is extremely low, typically in the range 0.1-1 $Wm^{-1}K^{-1}$,[7] approaching the low limit of thermal conductivity of inorganic thermoelectric materials; and electronic structures of organic (semi)conductors can be tuned through multiple methods of molecular chemistry.[8,9] Therefore, organic thermoelectric materials have potential applications at low temperatures.

1.2 Organic thermoelectric materials

The majority of organic thermoelectric materials reported are based on conductive polymers, including conjugated polymers and certain coordination polymers due to the great flexibility, tunable electronic structure (energy levels) and solution processability.

1.2.1 Conductive polymers

Since the discovery of metal-like behaviors in highly doped polyacetylene (PA) films, the conjugated polymers have been developed in thermoelectric study.[10,11] Increasing power factor (PF) through increasing carrier concentration by doping has been the major strategy for enhancing *ZT* of conductive polymers since their thermal conductivities are usually as low, and doping levels are mostly used to reflect the conductive properties of the conductive polymers. Electrochemical and chemical doping methods (redox reactions) have been used to tune the doping levels of the conjugated polymers, PA, polypyroles (PPr), polythiophenes (PTh), polyanilines (PANi) and poly(3,4-ethylenedioxythiophene) (PEDOT) to achieving higher carrier concentration to develop high power factor.[12] Generally, undoped conjugated polymers exhibit semiconducting properties, while oxidized or doped conjugated polymers can become conducting polymers because they are similar to doped semiconductors or metals. In the doping process, the conjugated polymers are exposed to the "dopant" by being dipped into the solution or gas containing an oxidizing agent. The polymers will be oxidized while the dopant will be reduced and changed into the negative counterion, anion, neutralizing the positive charges incorporated in the π-electron system of the conjugated polymers. Finally, conducting polymers can directly be synthesized in the oxidized form by chemical polymerization or electropolymerization with controllable

doping levels towards great conducting properties.[13] In some case, undoping or decreasing the oxidation level starting from a highly oxidized polymer can be realized through the electrochemical or chemical reaction by using a reducing agent.[8]

Highly doped conducting polymers are generally insoluble. The common strategy for enhancing solubility is forming a micelle-like dispersion by introducing a soluble counterion (polystyrene sulfonate (PSS) for PEDOT, PEDOT-PSS) or an ionic surfactant serving as a counterion for charge balance.[14] PEDOT:PSS is the most popular conducting polymer because it shows higher electrical conductivity by several orders of magnitude when a specific second solvent, such as ethylene glycol (EG) or dimethyl sulfoxide (DMSO), is added for "secondary doping". This is because the high boiling point solvents work for better polymer chain organization to enhance the conductivity, and this is called "morphology effect".[15,16] A maximum *ZT* value of 0.42 was obtained in DMSO treated PEDOT: PSS.[17] Furthermore, PEDOT:PSS is commercially available. In addition, in situ synthesized PEDOT:tosylate (tos) by using $Fe(tos)_3$ as an oxidant has also been widely studied for thermoelectric development due to its easy processability and high electrical conductivity (over 1000 S cm^{-1}) arising from the replacement of insulating polyanion phases with small-molecule anion phases, and a high *ZT* of 0.25 was obtained.[8] **Figure 1.2** gives molecular structures of PEDOT, PSS and tosylate (tos). **Table 1.1** shows thermoelectric results of some conducting polymers with power factor (PF) above 100 μW m^{-1} K^{-2} around 300 K.

Recently, thermoelectric properties of coordination polymers (poly[Ax (M-ett)]) were studied.[18] Metal coordination polymers have both n- and p-type forms with Ni (poly[Na_x(Ni-ett)] and poly[K_x(Ni-ett)]) and Cu (poly[Cu_x(Cu-ett)]) as coordinating atoms, respectively. The n-type polymer poly[K_x(Ni-ett)]) showed remarkable performance with high electrical conductivity (~60 S cm^{-1} at 440 K) and Seebeck coefficients (-150 μV K^{-1} at 440 K) and low thermal conductivity. As a result, the *ZT* values of poly[Na_x(Ni-ett)] and poly[K_x(Ni-ett)] were 0.1 and 0.2 at 440 K respectively, and poly[K_x(Ni-ett)] is the most efficient n-type organic thermoelectric material. The sign of Seebeck coefficient could be tuned by changing metal ions: the sign was negative for poly[Na_x(Ni-ett)] and poly[K_x(Ni-ett)] (n-type) but positive for poly[Cu_x(Cu-ett)] (p-type) with a *ZT* of 0.014 at 380K.

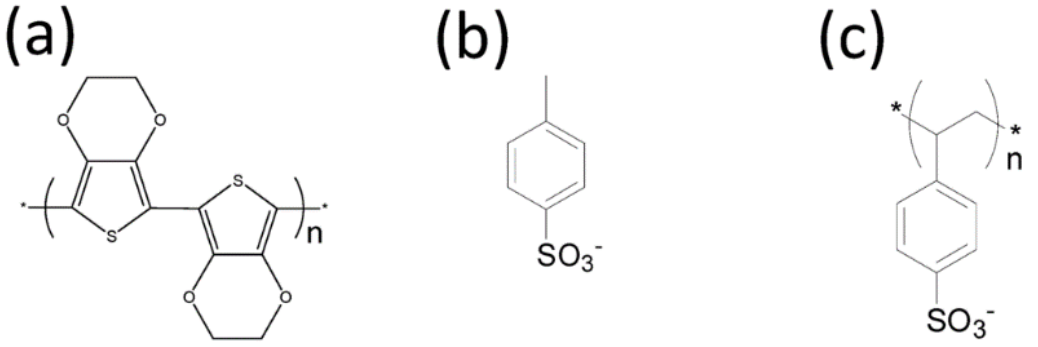

Figure 1.2 Molecular structures of (a) poly(3,4-ethylenedioxythiophene) (PEDOT), (b) tosylate (tos), and (c) poly(styrenesulfonate) (PSS).[19]

Table 1.1 Thermoelectric results of some conducting polymers with power factor (PF) above 100 μW m^{-1} K^{-2} around 300 K.[6]

Conducting polymers	Polymers with PF above 100 μW $m^{-1}K^{-2}$ around 300K				
	σ(S cm^{-1})	S(μV K^{-1})	PF(μW $m^{-1}K^{-2}$)	κ(W $m^{-1}K^{-1}$)	Treatment
PA:I_x	11110	28.4	900	0.69 (steady sate)	As-synthesized
PA:$FeCl_4$	7530	15.3	180	/	As-synthesized
PEDOT:Tos	238	40	38	/	As-synthesized (36%)
	80	200	324	0.33	TDAE-reduced
PEDOT:Tos	1354	79.7	861	/	As-synthesized (24%)
	923	117	1270	/	Electrochemically reduced
PEDOT:PSS (Clevios PH1000)	639	27.3	47.6	0.23 (0.52)	Spin-cast, EG
	620	33.4	69.2	0.24 (0.42)	Spin-cast, DMSO
	830	60	300	0.23 (0.37)	EG treated
	957	70	469	0.22 (0.31)	DMSO treated
PEDOT-C6:ClO_4	180	30	16	/	As-synthesized
	335	103	354.7	/	Electrochemically reduced

[a)] Cross-plane thermal conductivity values with in-plane conductivity included in brackets; [b)] Doping levels experimentally determined are enclosed in brackets.

1.2.2 Polymer nanocomposites

Polymer nanocomposites as thermoelectric materials possess advantageous characteristics from both polymer matrix and nano-fillers: low thermal conductivity, good solution processability and flexibility of polymers, together with the high power factor of nano-fillers. Among various nano-fillers, carbon nanotubes (CNTs) are recognized as one of the most effective fillers to enhance the electrical conductivity of the polymer matrix due to their extremely great charge transport properties.[20] The method of blending nano-fillers with the polymer matrix is often utilized to prepare polymer–CNT nanocomposites. A low content of CNTs in the composite is crucial to realize a high electrical conductivity without inducing a high thermal conductivity in the composite. For example, CNTs can form a three dimensional (3D) network structure within an insulating poly(vinyl acetate) (PVAc) matrix. The Seebeck coefficient (40–50 mV K^{-1}) and low thermal conductivity (0.2–0.3 W m^{-1} K^{-1}) were almost constant with the proper addition of CNTs, thus resulting in the best ZT of 0.006 at a CNT concentration of 20 wt% at 300 K.[21] This is because the connecting junctions between CNT and polymers in nanocomposites play an important role in enhancing the electrical conductivity without increasing the thermal conductivity of polymer–CNT nanocomposites. As is shown in **Figure 1.3**, when CNTs are blended in a polymer matrix, junctions will be formed between CNTs and polymers, which is called interfaces. Due to the mismatch of the molecular vibrational spectra between polymers and CNTs, the phonon transport will be impeded at the interface. When the insulating PVAc matrix is replaced with conductive polymer PEDOT:PSS, the maximum electrical conductivity of nanocomposites is greatly increased from 48 S cm^{-1} in PVAc–CNT nanocomposites to 1350 S cm^{-1} in PEDOT:PSS–CNT nanocomposites, while the Seebeck coefficient and thermal conductivity were almost retained, respectively.[22] The interface can also generate the energy-filtering effect to decouple the correlated parameters of Seebeck coefficient and electrical conductivity. This is due to that appropriate boundary barriers preferentially allow the high-energy carriers to pass, which can increase the mean carrier energy that flows through the polyaniline–CNT interface and lead to an increased Seebeck coefficient.[23]

It should be noted that one of the most attractive characteristics of polymer–inorganic thermoelectric nanocomposites is the synergetic combination of the easy processability

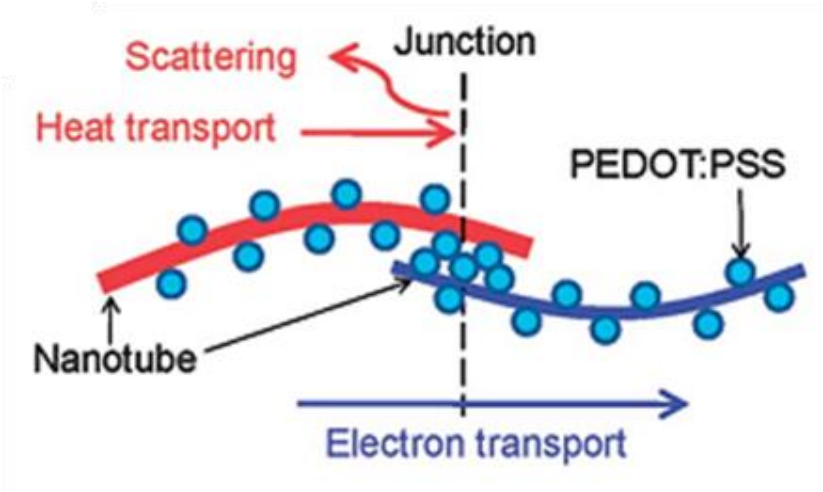

Figure 1.3 Schematic illustration of the junctions at PEDOT:PSS–CNT interface in the nanocomposites.[22]

of polymers and the excellent thermoelectric performance of inorganic nanostructures. Among the inorganic semiconductors, Bi, Te, and Bi_2Te_3 nanostructures are mostly used to produce polymer nanocomposites due to their high power factor at room temperature and easy fabrication.[24] Recently, the best ZT of polymer–inorganic nanocomposites have been observed in PEDOT:PSS–Te nanorod composites, ZT of 0.1 at 300 K.[25] The in-situ prepared nanocomposites exhibited a higher power factor than those of individual components and a low thermal conductivity comparable to that of the polymer matrix due to the continuous electrical network and the energy-filtering effect at polymer–inorganic interfaces. The semiconducting polymer, P3HT (poly(3-hexylthiophene-2,5-diyl)), is also widely used in polymer–inorganic thermoelectric nanocomposites. For example, it has been further investigated that the organic–inorganic semiconductor interface in polymer–inorganic nanocomposites can also act as an energy-filter by utilizing the P3HT–Bi_2Te_3 nanocomposites with P3HT of different doping levels (by $FeCl_3$) as matrix.[26] As shown in **Figure 1.4**, by controlling the doping levels, the interfacial potential barrier can be tuned to work for the energy-filtering effect to selectively allow high-energy carriers to flow to enhance Seebeck effect and power factor.

1.3 The current situation and our device design

The Seebeck coefficient, *S*, is a critical parameter to determine the thermoelectric efficiency given by the dimensionless figure-of-merit $ZT=(S^2\sigma/\kappa)T$. Theoretically, the Seebeck effect originates from charge (electrons or holes) diffusion caused by the entropy difference in internal energies of charge carriers between the hot and cold surfaces in a material and is determined by the electronic structure and scattering of charge carriers.[27,28] In order to obtain a high figure of merit, as mentioned in the previous parts, various methods have been used to increase the carrier concentration to increase the electrical conductivity of the materials. However, it inevitably decreases the Seebeck coefficient of the organic film due to the increased carrier concentration. Generally, increasing charge density leads to a decrease in entropy difference across a

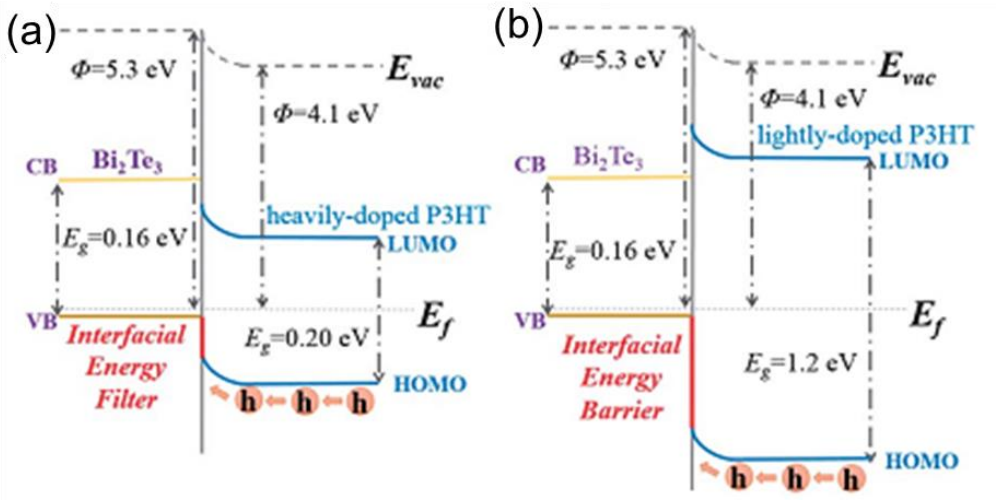

Figure 1.4 The band diagram of P3HT–Bi_2Te_3 interface based on (a) the heavily doped P3HT matrix and (b) the lightly doped P3HT matrix.[26]

given section and an increased electronic contribution to the thermal conductivity, both of which are undesirable for thermoelectric applications.[29-31] This decrease in entropy difference diminishes the Seebeck effect, making it necessary to find an additional driving force for charge diffusion. The multi-layer conductor/organic/conductor thin-film devices can exhibit a high Seebeck effect due to allowed electrical conduction and limited thermal conduction across the organic film between two conductor surfaces.[32] With this vertical multi-layer thin film design a low temperature difference can generate a large temperature gradient to develop Seebeck effect in intermediate temperature ranges. In particular, the multi-layer conductor/organic/conductor thin-film devices provide the possibilities of exploring additional driving force to develop Seebeck effect by using temperature-dependent surface polarization. It is noted that the surface of an organic film can exhibit a temperature-dependent polarization, well-known as temperature-dependent dielectric polarization,[33-37] through electron-phonon coupling mechanism.[12, 38 , 39] Upon applying a temperature difference, the high and low-emperature conductor/organic interfaces can show stronger and weaker polarizations, establishing a temperature-dependent built-in field from high to low-temperature surface in the vertical multi-layer conductor/organic/conductor devices. This temperature-dependent built-in field can drift positive and negative carriers towards low and high-temperature surfaces, respectively, leading to a positive Seebeck effect on both electron and hole transport. Therefore, the surface-polarization difference can present as a new driving force to develop Seebeck effect in the vertical multi-layer conductor/organic/conductor devices. On the other hand, a temperature difference can still generate an entropy difference in the internal energy of charge carriers between high and low-temperature surfaces. This entropy difference diffuses both negative and positive carriers from high to low-temperature surface, generating negative and positive Seebeck effect based on electron and hole diffusion.[40-45] Therefore, we can propose that the vertical multi-layer conductor/organic/conductor thin-film devices can combine Seebeck effect generated by both surface-polarization and entropy differences.

Chapter 2

2 Surface polarization enhanced Seebeck effects in vertical multi-layer metal/polymer/metal thin-film devices

2.1 Introduction

The entropy difference[46,47] has been heavily used as the driving force to diffuse charge carriers between high and low temperature surfaces towards the development of Seebeck effects in thermoelectric devices. Specifically, the high and low temperature surfaces exhibit different internal energies of charge carriers in a medium, generating an entropy difference in carrier density of energetic charge carriers. This entropy difference initiates the diffusion of energetic charge carriers from high to low temperature surface and consequently generates an electrical voltage in the development of Seebeck effects. The entropy difference in internal energy of charge carriers has been serving as the main driving force behind the Seebeck effects in bulk materials. However, this driving force from entropy difference can cause an inverse relationship between Seebeck coefficient and electrical conductivity in the thermoelectric developments. We can see in Eq. (1) that increasing the charge density can lead to a decrease on the Seebeck coefficient developed by the entropy difference. Here, the Seebeck coefficient can be given by:

$$S = \frac{\Delta W}{\Delta n} = \frac{k_B}{e}(\ln(\frac{N_c}{n}) + A) \quad (1)$$

where ΔW is the entropy difference across high and low temperature surfaces, Δn is the charge flow through a given section, k_B is the Boltzmann constant, e is electron charge, N_c is the effective density of states, n is the carrier concentration, and A is the carriers' kinetic energy normalized to k_BT. Clearly, increasing the charge density for boosting electrical conductivity can negatively affect the Seebeck coefficient. This is because increasing the charge density can decrease the entropy difference to diffuse the charge carriers at a given temperature gradient. Therefore, it is necessary to develop a new driving force, additional to entropy difference, for the diffusion of charge carriers to

eliminate the negative effects caused by increased carrier concentration toward developing high Seebeck effects.

In this study, we explore temperature-dependent surface polarization, as a new driving force, for developing Seebeck effects based on vertical metal/polymer/metal thin-film devices. In general, a hybrid metal/polymer interface can be used to restrict the thermal conduction but to allow the electric conduction.[48-57]Here, the vertical thin-film design provides the possibility of developing temperature-dependent surface polarization for the development of Seebeck effects. The temperature-dependent surface electrical polarization can come from the following two effects. First, the coupling between local polarization and thermal vibration can directly cause the temperature-dependent polarization through charge-phonon coupling mechanism. In fact, it has been found that the charge-phonon coupling can increase the Seebeck effect in the horizontal direction along polymer films.[38,58,59]Second, the interfacial dipoles modulated by the thermally activated Fermi electrons on the metal surfaces can also contribute to the temperature-dependent polarization. These two effects combine to generate a difference in electrical polarization, namely temperature-dependent built-in electric field, across the polymer film between high and low-temperaturemetal surfaces.This temperature-dependent built-in electric field established by the surface polarization can drive the diffusion of charge carriersfor the development of Seebeck effects. To enhance the temperature-dependent surface polarization, a high dielectric layer can be inserted at the metal/polymer interface, increasing the built-in electrical field between high and low-temperature surfaces.[60-62]The inserted dielectric interface can also allow theelectrical conduction through transport but further hinder the thermal conduction through interface phonon scattering. In our study, the high dielectric film (MoO_3, dielectric constant~40)[63] was selected to enhance the temperature-dependent surface polarization in the vertical metal/dielectric/polymer/metal thin-film devices.

2.2 Experimental

The hybrid organic/inorganic thin-film thermoelectric devices were fabricated with the sandwiched metal/polymer/metal architecture. Two specific types of thermoelectric devices were used, with and without the high dielectric MoO_3 film: Al/MoO_3/P3HT:PCBM/Al and Al/P3HT:PCBM/Al, in our experiments. The fabrication processes are shown below. A 50 nm thick aluminum (Al) layer was thermally evaporated onto a glass substrate to form a bottom metal film. An 8 nm thick MoO_3 layer was then evaporated on top of the Al layer for the devices with the dielectric interface. The P3HT:PCBM films were then spin-cast with the thickness of about 250nmon top of the previous layers under nitrogen atmosphere. The P3HT:PCBM composite was prepared in chloroform with the weight ratio 10:1, which can lead to a p-type thin film. The top Al film was then evaporated with 50 nm thickness on top of the P3HT:PCBM film. The thermal evaporations were performed under the vacuum of $4x10^{-6}$ Torr. The Poly(3-hexylthiophene) (P3HT) and [6,6]-phenyl(C61-butyric) acid (methylester) (PCBM) were purchased from Rieke Metals and Nano-C, respectively. The MoO_3 was purchased from Sigma-Aldrich. To obtain Seebeck effect in the vertical direction of the multilayer thin-film thermoelectric devices, the K-type thermocouples and copper wires were connected to both bottom and top Al films to measure the temperature and electrical potential differences between the two Al surfaces, respectively. The hot plate was used to heat the bottom side of the device, namely hot surface of the hybrid metal/polymer/metal devices. The voltage and temperature differences were measured using an InstruNet Model 100 Input/Output System. The obtained data was used to calculate the Seebeck Coefficient, S ($S = \frac{\Delta V}{\Delta T}$), in which $\Delta V = V_{cold} - V_{hot}$ and $\Delta T = T_{hot} - T_{cold}$. The current density-voltage (*J*-*V*) measurements were performed to characterize the electrical conductivity of our hybrid thin-film thermoelectric devices by using Lab Tracer software along with a Keithley 2400 power supply. The capacitance-voltage (*C*-*V*) characteristics were measured at different temperatures using an impedance spectrometer (Agilent, E4980A) to explore

the temperature-dependent surface polarization.

2.3 Results and Discussions

The device structure is shown in **Figure 2.1**. The MoO_3 layer can enhance surface polarization for larger Seebeck and also improve the interface contact to enhance electrical conductivities of the device.

Figure 2.2 shows the schematic diagram for the temperature-dependent surface polarization in the development of Seebeck effects in the vertical metal/polymer/metal thin-film devices. The polymer film was prepared by using a blend containing a semiconducting polymer (P3HT) and PCBM. The P3HT matrix allows charge transport[38,64] while the PCBM decreases the thermal transport due to extremely low thermal conductivity.[65,66] The temperature-dependent surface polarization on the P3HT:PCBM film surfaces requires (i) the coupling between local electrical polarization and thermal vibration through charge-phonon coupling mechanism on the polymer surfaces and (ii) the interfacial dipoles at metal/polymer interface modulated by the thermally activated Fermi electrons on the metal surface. In general, organic semiconducting materials can exhibit a strong coupling between local polarization and thermal vibration.[67-70] This is because the delocalized π electrons can Coulombically interact with thermally vibrated molecular structures on a semiconducting polymer chain in a low dielectric background. The strong coupling between local polarization and thermal vibration can directly develop a temperature-dependent surface polarization on the P3HT:PCBM film surfaces, which can be experimentally evidenced by the well-known phenomenon: temperature-dependent dielectric constants in polymer materials. It has been observed that the dielectric constant for conjugated polymer DB-OPV (dibenzo 18-crown-6 ether ring substituted oligo (p-phenylenevinylene)) could increase from 2.5 to 7at fixed frequencies when the temperature changes from 30 ^{o}C to 60 ^{o}C.[71-75] Therefore, the strong coupling between local polarization and thermal vibration provides a mechanism to generate a temperature-dependent surface polarization as a new driving force, additional to entropy difference, to develop Seebeck effects.

$$Seebeck(S) = \frac{\Delta V}{\Delta T}$$

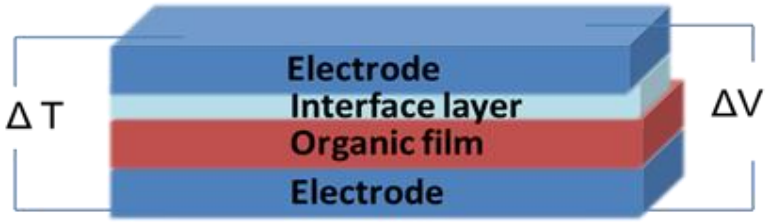

Figure 2.1 Structure of the vertical multi-layer Al/P3HT:PCBM/Al thin-film devices.

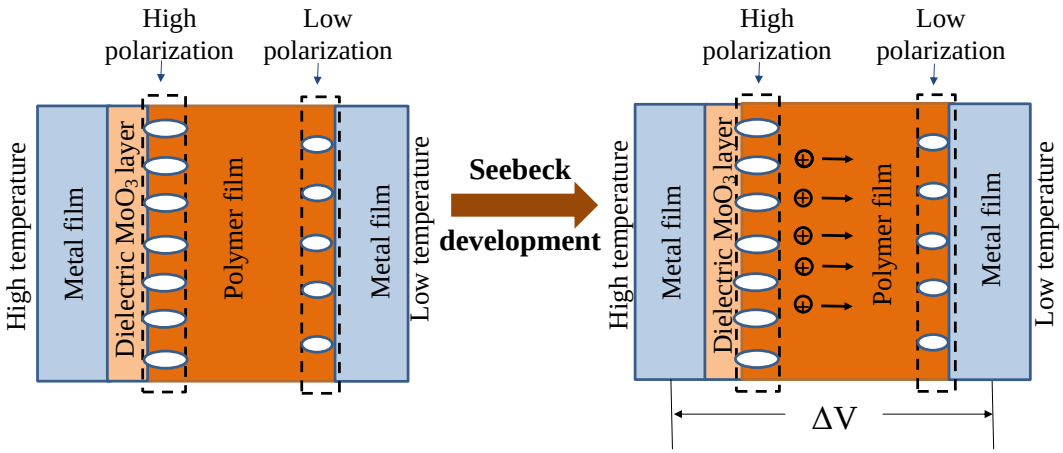

Figure 2.2 Schematic diagram to show the development of Seebeck effects driven by temperature-dependent surface polarization in the vertical metal/dielectric/polymer/metal thin-film device. The average temperature difference detected between the high temperature surface and the low temperature surface is around 1.2 ^{o}C.

On the other hand, the interfacial dipoles, formed at metal/polymer interface through charge transfer,[76,77] can be modulated by thermally activated Fermi electrons. This is because the Fermi electrons on the metal surface are accountable for the charge transfer or wave function hybridization towards the formation of interfacial dipoles at the metal/polymer interface. A higher temperature can thermally activated a larger number of Fermi electrons on the metal surface, as evidenced by temperature-dependent specific heat (C_{el}) from electron gas in metallic materials through the relationship: $C_{el} \sim N(E_F)T$, where $N(E_F)$ is the density of electron states at Fermi level, and T is temperature.[78] As a consequence, high and low temperatures can lead to stronger and weaker dipole moments at the metal/polymer interface respectively. This would lead to an electrical potential difference between the high temperature and low temperature surfaces in the vertical metal/polymer/metal thin-film devices. Clearly, both the coupling between local polarization and thermal vibration and the interfacial dipoles modulated by the density of surface Fermi electrons can lead to a temperature-dependent surface polarization, forming a temperature-dependent built-in electrical field as an additional new driving force, additionally to the entropy difference, to diffuse charge carriers from high to low-temperature surface towards the development of Seebeck effects.

We should note that the temperature-dependent surface polarization established through the coupling between local polarization and thermal vibration may provide a mechanism that allows the co-operative relationship between Seebeck coefficient and electrical conductivity. Within first-order approximation, we can assume that the coupling strength (β) between local polarization and thermal vibration is proportional to the charge density (n) and phonon density (p),

$$\beta = \alpha \cdot n \cdot p, \tag{2}$$

where α is the constant. The $\partial\beta/\partial T$ essentially determines the driving force for the development of Seebeck effects. At a given temperature gradient, we can see in Eq. (2) that increasing the charge density in boosting the electrical conductivity can indeed increase the coupling between local polarization and thermal vibration and consequently the temperature-dependent surface polarization. Therefore, using

temperature-dependent surface polarization can lead to a simultaneous enhancement on Seebeck coefficient and electrical conductivity in the vertical metal/polymer/metal thin-film devices.

Figure 2.3(a) shows Seebeck coefficients generated from two types of devices without and with high-dielectric MoO_3 thin layer, namely Al(hot)/P3HT:PCBM/Al(cold)and Al(hot)/MoO_3/P3HT:PCBM/Al(cold)devices, under completely dark condition. We can see that the Seebeck coefficients from these two devices exceed 680μVK^{-1} and 845μVK^{-1} at 80 ºC. We should note that the P3HT:PCBM blend film can exhibit low bulk-thermal conduction due to the extremely low thermal conductivity from PCBM component.[65,66] On the other hand, the P3HT:PCBM blend film can allow electrical conduction in thermoelectric developments.[38,64] **Figure 2.3(b)** shows that the thermovoltage (V) increases linearly with temperature (T) for both types of devices. We should note that the temperature-dependent polarization can generate two different phenomena: namely true and fake Seebeck effects in the vertical metal/polymer/metal devices when the electrical voltage is measured across the high and the low temperature surfaces. The true Seebeck effect requires the charge diffusion driven by the temperature-dependent surface polarization. The fake Seebeck effect can be generated without charge diffusion when the temperature-dependent surface polarization causes an electrical potential difference during the voltage measurement across the high and the low temperature surfaces. Here, we should note that a true Seebeck effect through charge diffusion can lead to a linear relationship between Seebeck coefficient (S) and temperature (T), as described by[79-82]

$$S \sim T \frac{d\ln\sigma(E)}{dE} | E_F \quad (3)$$

where $\sigma(E)$ is a conductivity-like function of electron energy E, and E_F is the Fermi energy.This linear relationship has been observed in many semiconducting polymers for thermopower developments.[38,39,79-82] In our work, we can see in Figure 2.3b that the Seebeck coefficient can indeed linearly increase with temperature. This confirms that our Seebeck effect is a true thermoelectric phenomenon developed by the charge diffusion driven by temperature-dependent surface polarization. In addition, we should

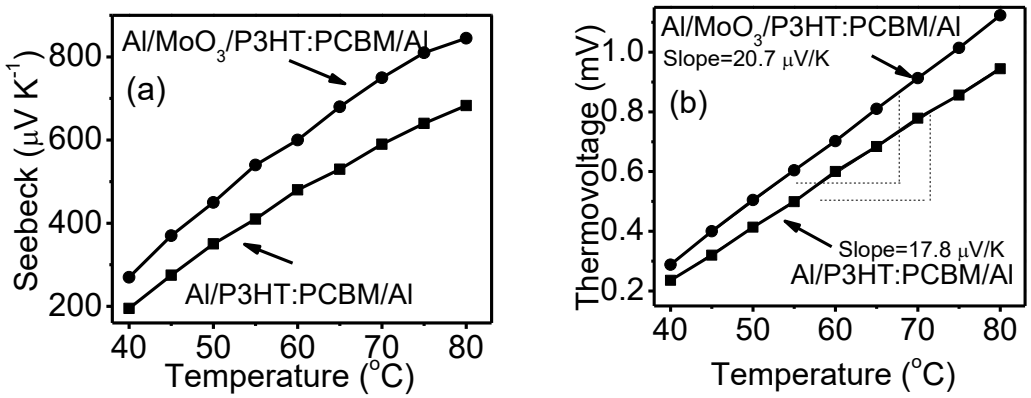

Figure 2.3 (a): Seebeck effect and (b): thermovoltage with increasing temperature for thermoelectric Al/P3HT:PCBM/Al and Al/MoO_3/P3HT:PCBM/Al devices.

point out that our vertical metal/polymer/metal devices are sensitive to small temperature differences due to the large temperature gradient (ΔT/thickness) across the polymer thin-film. We cans see in Figure 2.3(a) that a small temperature difference (~ 1.2°C) can lead to a large Seebeck coefficient. However, if a large temperature difference is used, the Seebeck effect can be decreased. This phenomenon suggests that a large temperature difference corresponds to a significant temperature gradient across the polymer film and consequently increases the heat transfer from high to low temperature surface through thermal radiation mechanism. This can essentially decrease the Seebeck effect in our vertical metal/polymer/metal thin-film devices. Nevertheless, our vertical metal/polymer/metal thin-film devices present a uniqueness: a small temperature difference can generate a large Seebeck effect.

Here, we should note that the Seebeck coefficient and thermovoltage from Al/MoO_3/P3HT:PCBM/Al are relatively larger than that from the device without the dielectric layer within the entire temperature range from 40°C to 80°C. In other words, the dielectric MoO_3 interface layer causes an increase on the Seebeck coefficient and thermovolatge in the Al/MoO_3/P3HT:PCBM/Al thin-film device. Especially, as shown in Figure 2.3(b), the slope of thermovoltage versus temperature from the device with the dielectric layer (MoO_3) is slightly larger than that without the dielectric, which means that thermovoltage of the device with the dielectric layer (MoO_3) is increased more quickly with temperature than that without the dielectric layer. We should note that the high dielectric MoO_3 layer can exhibit a strong surface polarization which can interact with the surface polarization of polymer layer at the MoO_3/P3HT:PCBM interface and consequently increases the coupling between local polarization and thermal vibration on the polymer surface. The increased coupling between local polarization and thermal vibration on polymer surface can then generate a stronger temperature-dependent surface polarization in the Al/MoO_3/P3HT:PCBM/Al device. A stronger temperature-dependent surface polarization provides a higher built-in electric field between high and low-temperature surfaces in the development of Seebeck effects. Therefore, using a high dielectric interface layer can lead to an enhancement on Seebeck effects through temperature-dependent surface polarization, as shown in

Figure 2.3(a).On the other hand, the dielectric interface layer can still serve the purpose of restricting thermal conductivity through phonon scattering at interfaces,[83,84] and it has been also found that the dielectric MoO_3 layer can enhance the electrical conductivity in organic thin-film devices by reducing interfacial contact resistance and facilitating charge transport.[85-88]

Here we use capacitance-voltage (C-V) measurements to experimentally analyze the temperature-dependent surface polarization in our vertical thin-film thermoelectric devices. Essentially, measuring the device capacitance can reflect the surface polarization of polymer layer through dielectric polarization in the vertical metal/polymer/metal thin-film devices.[89,90] Figure **2.4**(a) and (b) show the *C-V* characteristics for Al/P3HT:PCBM/Al and Al/MoO_3/P3HT:PCBM/Al devices at different temperatures under dark condition. We can see that both these two devices show a bias-dependent capacitance in dark condition, thus indicating field-dependent surface polarization. At zero bias the device with the dielectric MoO_3 layer shows a larger capacitance and thus a stronger surface polarization than that without the MoO_3 layer. In particular, the capacitance for both devices increases with increasing temperature. The temperature dependence of capacitance provides an experimental argument that the dielectric constant changes with temperature on the polymer surfaces in the vertical metal/polymer/metal thin-film devices. The temperature-dependent dielectric constant can then generate the temperature-dependent surface polarization in the development of Seebeck effects. We should point out that mobile charges can also cause temperature-dependent surface polarization in the metal/polymer/metal devices. To clarify this issue, we have compared different organic materials (P3HT:PCBM, MEHPPV, and PEDOT) with different mobile charges. Our temperature-dependent capacitance measurements clearly indicate that the observed temperature-dependent capacitance is mainly from temperature-dependent polarization effects, not much related to mobile charges in our devices. This is because the mobile charges, even if they exist, cannot appreciably respond to the applied AC bias of 50 mV in the capacitance measurements, and do not play an important role in our measurements.[91] Therefore, our capacitance measurements are mainly related to polarization effects. Our

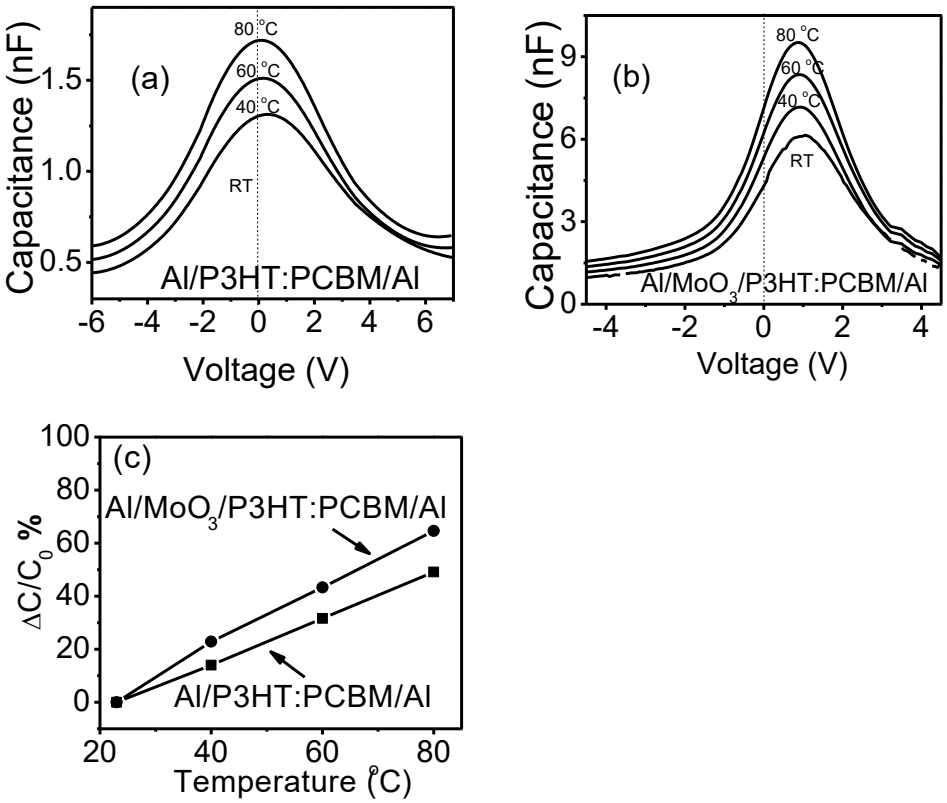

Figure 2.4 (a):Capacitance-voltage (C-V) characteristics at different temperatures for thermoelectric devices Al/P3HT:PCBM/Al; (b):C-V characteristics at different temperatures for Al/MoO_3/P3HT:PCBM/Al; c:the percent change of capacitance at zero bias ($\Delta C/C_0 = (C-C_0)/C_0$, where C_0 is the capacitance at zero bias at room temperature and C is the capacitance at zero bias at high temperature) is shown as a function of temperature for both types of devices.

experimental observation provides an evidence that the temperature-dependent surface polarization exists in both Al/P3HT:PCBM/Al and Al/MoO_3/P3HT:PCBM/Al devices. More importantly, increasing temperature from room temperature to 80ºC increases the zero-bias capacitance from 1.15 nF to 1.70 nF by 48 % for the Al/P3HT:PCBM/Al device, but from 4.3nF to 7.1 nF by 65 % for the Al/MoO_3/P3HT:PCBM/Al device (Figure 2.4(c)). Clearly, the device with the dielectric MoO_3 layer shows a larger change in capacitance with increasing temperature than that without the dielectric layer. These *C*-*V* results confirm that the high dielectric MoO_3 layer can indeed enhance the temperature-dependent surface polarization and consequently provides a stronger driving force, in addition to entropy difference, to develop Seebeck effects in the vertical metal/polymer/metal thin-film devices.

Electrical conduction is also an important parameter in the development of Seebeck effects in the vertical metal/polymer/metal thin-film devices. The high dielectric MoO_3thin film is known as charge transporting layer which can increase the electrical conduction in organic thin-film devices.[86,87] The current density-voltage (*J*-*V*) characteristics (Figure4) are used to approximate electrical conduction by using Cheung's method:[92-94]

$$\frac{dV}{d(lnJ)} = constant + R * A * J \quad (4)$$

where *V* is voltage, *J* is current density, *R* resistance, and *A* area of the device. We can see in **Figure 2.5(a)** that the device with the dielectric MoO_3 layer (Al/MoO_3/P3HT:PCBM/Al) shows stronger charge injection and transport than the device without the dielectric MoO_3 layer (Al/P3HT:PCBM/Al). We can see from the **Figure 2.5(b)** that the devices with and without the dielectric MoO_3 layer show the electric conductivities of 0.9E-5 Sm^{-1} and 1.4E-8 Sm^{-1},respectively, by using Cheung's method. It can be seen that Al/MoO_3/P3HT:PCBM/Al has much larger electrical conductivity (0.9E-5 Sm^{-1}) compared with Al/P3HT:PCBM/Al (1.4E-8Sm^{-1}). Clearly, using the dielectric MoO_3 layer can increase the electrical conductivity in the hybrid thin-film device. This can be attributed to the fact that the dielectric layer, MoO_3, can

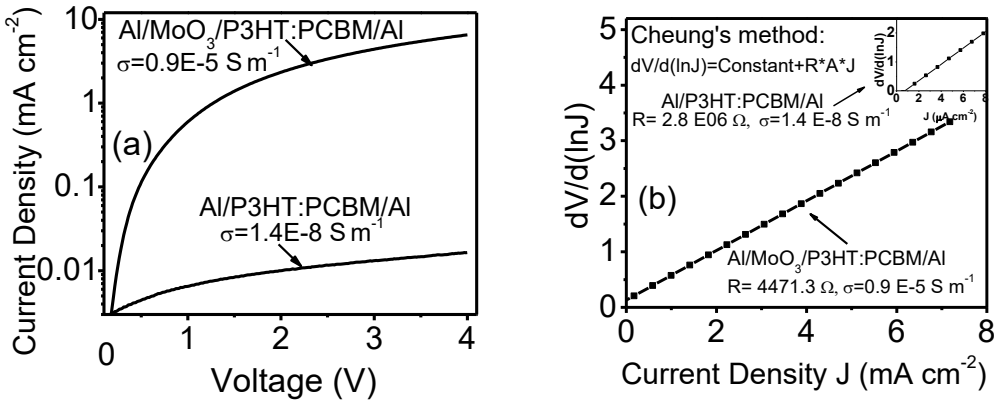

Figure 2.5 (a):Current density-voltage curves for the thermoelectric devices with and without dielectric MoO_3 layer; (b): Calculated electrical conductivities ($\sigma = L/(R*A)$, where L is film thickness, R calculated resistance by using Cheung's method, and A contact area) for the devices with and without dielectric MoO_3 layer.

reduce the interfacial contact resistance and enhances the charge transport in the vertical metal/polymer/metal thin-film thermoelectric devices.[95,96] Therefore, using dielectric layer provides a possibility that both Seebeck coefficient and electrical conductivity can be simultaneously enhanced towards the development of higher power factor, $S^2\sigma$, based on the vertical metal/polymer/metal thin-film design.

2.4 Conclusion

In summary, temperature-dependent surface polarization was explored as an additional driving force to diffuse charge carriers from low to high-temperature surface towards the development of high Seebeck effects based on vertical metal/polymer/metal thin-film devices. We obtained enhanced Seebeck effects by using a high-dielectric MoO_3 layer through increasing the temperature-dependent polarization within the Al/MoO_3/P3HT:PCBM/Al thin-film device. Simultaneously, the electrical conductivity was also increased when the high-dielectric MoO_3 layer was used in the thin-film device. Therefore, using the high dielectric layer provides a possibility to cooperatively enhance the Seebeck coefficient and electrical conduction in organic materials.

Chapter 3

3 Exploring tunable Seebeck regimes between entropy and polarization differences by controlling electrical conductivity based on vertical multi-layer electrode/organic/electrode thin-film devices

3.1 Introduction

The multi-layer conductor/organic/conductor thin-film devices can exhibit a high Seebeck effect due to allowed electrical conduction and limited thermal conduction across the organic film between two conductor surfaces. [97-99] With this vertical multi-layer thin film design a low temperature difference can generate a large temperature gradient to develop Seebeck effect in intermediate temperature ranges. In particular, the multi-layer conductor/organic/conductor thin-film devices provide the possibilities of exploring additional driving force to develop Seebeck effect by using temperature-dependent surface polarization. It is noted that the surface of an organic film can exhibit a temperature-dependent polarization, well-known as temperature-dependent dielectric polarization, [100 - 104] through electron-phonon coupling mechanism. [105 - 107] Upon pplying a temperature difference, the high and low-temperature conductor/organic interfaces can show stronger and weaker polarizations, establishing a temperature-dependent built-in field from high to low-temperature surface in the vertical multi-layer conductor/organic/conductor devices. This temperature-dependent built-in field can drift positive and negative carriers towards low and high-temperature surfaces, respectively, leading to a positive Seebeck effect on both electron and hole transport. Therefore, the surface-polarization difference presents as a new driving force to develop Seebeck effect in the vertical multi-layer conductor/organic/conductor devices. On the other hand, a temperature difference can still generate an entropy difference in the internal energy of charge carriers between high and low-temperature surfaces. It is known that this entropy difference diffuses both positive and negative carriers always from high to low-temperature surface, generating negative and positive Seebeck effect based on electron and hole diffusion. [108 - 117] Essentially, the vertical multi-layer conductor/organic/conductor thin-film devices combine Seebeck effect generated by both surface-polarization and entropy differences. In n-type organic materials, entropy

and polarization differences generate negative and positive Seebeck coefficients, respectively. As a result, using the n-type organic material design presents as a convenient method to identify the tunable Seebeck regimes between surface-polarization and entropy difference. In this work we explore the possibilities of tuning Seebeck effect between surface-polarization and entropy regimes by using n-type organic materials: PCBM ([6,6]-phenyl(C60-butyric) acid (methyl ester)) and CN-MBE (1-cyano-1,2-bisbiphenyl-ethylene) [118] based on the vertical thin-film device design of ITO/organic/Au. The selected n-type organic materials possess strong temperature-dependent surface polarization at conductor/organic interface. We find that changing electrical conductivity can essentially tune the Seebeck effect between surface-polarization and entropy regime in the vertical multi-layer conductor/organic/conductor thin-film devices.

3.2 Experimental

The hybrid organic/inorganic thin-film thermoelectric devices were fabricated with the sandwiched electrode/organic/electrode architecture. Two specific types of thermoelectric devices were used in our experiments: ITO/PCBM:PMMA composite/Au and ITO/CN-MBE/Au. The PCBM:PMMA composite and CN-MBE solutions were prepared in chloroform. These solutions were spin-cast with thicknesses of about 200 nm on top of clean ITO electrodes under a nitrogen atmosphere. The films were then annealed for 15 min under a nitrogen atmosphere. The top Au film was then evaporated with a thickness of 50 nm on top of the organic films under a vacuum of 2.6×10^{-6} Torr. The [6,6]-phenyl(C60-butyric) acid (methyl ester) (PCBM) was purchased from Nano-C. The PMMA was purchased from Aldrich. The CN-MBE was synthesized in Seoul National University, South Korea. To obtain the Seebeck effect in the vertical direction of the multilayer thin-film thermoelectric devices, K-type thermocouples and copper wires were connected to both the bottom ITO and top Au electrodes to measure the temperature and electrical potential differences between the two electrode surfaces, respectively. A hot plate was used to heat the bottom side of the device, namely the hot surface of the hybrid electrode/organic film/electrode devices. The voltage and temperature differences were measured using an InstruNet Model 100

Input/Output System. The obtained data was used to calculate the Seebeck coefficient, S ($S = \frac{\Delta V}{\Delta T}$), in which $\Delta V = V_{cold} - V_{hot}$ and $\Delta T = T_{hot} - T_{cold}$. The temperature difference between the high-temperature and the low-temperature surfaces is around 1°C.

3.3 Results and Discussions

Figure 3.1(a) and (b) show Seebeck effects and electrical conductivities in vertical thin-film thermoelectric devices based on n-type PCBM. Photoexcitation is used to increase the electrical conductivity. The Seebeck coefficients from the n-type PCBM film go from positive values in the dark condition to negative values under photoexcitation. In the dark condition, the Seebeck effect is developed by the driving force of surface polarization through the charge-phonon mechanism, which leads to positive Seebeck coefficients. Using photoexcitation generates sufficient free charge carriers for diffusion under a temperature difference, leading to negative Seebeck coefficient values driven by entropy difference under a temperature difference. This indicates that by tuning the electrical conductivity through changing charge concentration, the Seebeck effect can be modulated from the surface polarization regime to the entropy difference regime for development of the thermoelectric effect.

Figure 3.2(a) shows Seebeck coefficients of ITO/PCBM:PMMA/Au devices with varying compositions under increasing temperatures. PMMA is used to modulate the electrical conductivity (σ) of the film of PCBM:PMMA composites. The device based on the pure PCBM film shows positive Seebeck coefficients. With 30 wt% PMMA in the composite, the Seebeck coefficients become negative with increasing temperatures. By further increasing the weight ratio of PMMA in the composite, at 50 wt% PMMA in the PCBM:PMMA composite, the Seebeck coefficients go back to positive values from negative values. The positive Seebeck coefficients of pure PCBM and PCBM:PMMA(50 wt%) films can be attributed to the polarization regime with low electrical conductivities. Essentially, the surface-polarization difference, caused by electron-phonon coupling on conductor/organic interface, establishes a temperature-dependent built-in field from high to low-temperature surface, drifting the negative

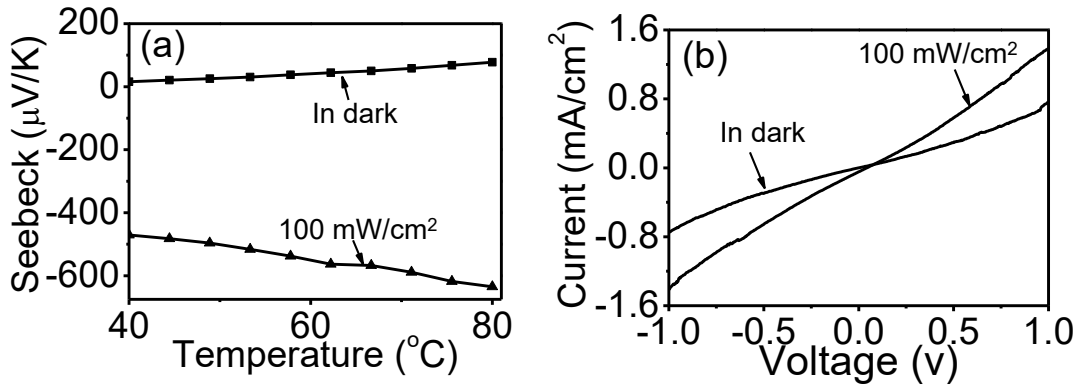

Figure 3.1 (a) Seebeck effects and (b) electrical conductivity in vertical thin-film thermoelectric devices based on n-type PCBM using photoexcitation (100 mW/cm^2) to increase electrical conductivity.

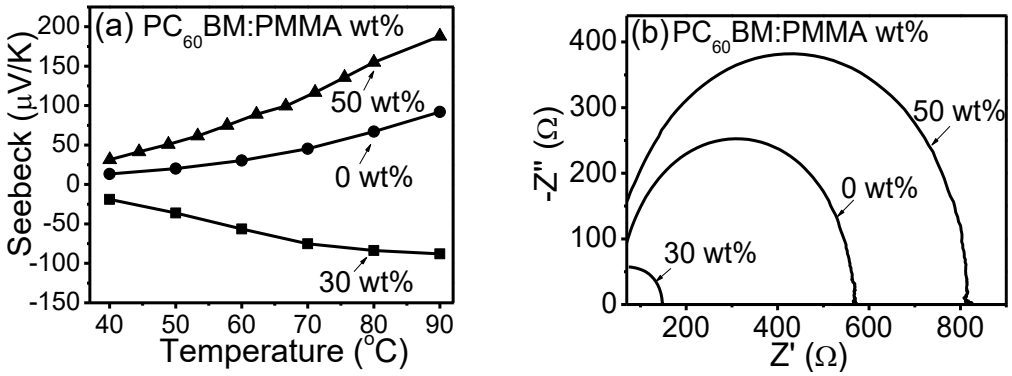

Figure 3.2 (a) Seebeck effect and (b) Cole-Cole curves in vertical thin-film thermoelectric devices: ITO/PCBM:PMMA/Au, with varying wt% of PMMA.

carriers from low to high-temperature surface.[97-99] This generates a positive Seebeck effect in the n-type conductor/organic/conductor devices. While, the negative Seebeck coefficients of the PCBM:PMMA(30 wt%) can be attributed to the domination of entropy regime (high electrical conductivities). Within this regime, the driving force of entropy difference could drive the diffusion of negative carriers from high to low-temperature surface, generating negative Seebeck coefficients in n-type devices.

Here, composition-dependent electrical conductivity of the ITO/PCBM:PMMA/Au thin-film devices is characterized by Cole-Cole curves, as shown in Figure 3.2(b). The Cole-Cole characteristics were measured using an impedance spectrometer (Agilent, E4980A). The Cole-Cole equation is generally defined as

$$Z = R + iX \quad (1)$$

where the complex Z contains the real part, resistance (R), and the imaginary part, reactance (X). The resistance can include both bulk resistance and interfacial resistance.[119 - 122] Here, we use the resistance value at X=0 to reflect the device resistance by changing the composition. By increasing the weight ratio of PMMA in the PCBM:PMMA film, the electrical conductivities first increase then decrease. At 30 wt% PMMA in the PCBM:PMMA film, the electrical conductivity is increased compared with pure PCBM, which can be attributed to the improved charge carrier transport by the increased charge mobility when PCBM molecules are incorporated in the PMMA polymer matrix. The Seebeck effect exhibits negative values at 30 wt% PMMA in the composite with increasing temperatures. By further increasing the PMMA weight ratio in the composite, at 50 wt% PMMA in PCBM:PMMA film, the electrical conductivity is greatly decreased. This is due to that PMMA is an insulating polymer, and with more PMMA in the composite the carrier conduction would be obviously decreased. The Seebeck effect is then switched to positive values. Clearly, changing the electrical conductivity can tune the major driving force of developing Seebeck effect between surface polarization and entropy difference under a temperature difference. For the devices with lower electrical conductivities, the surface polarization from charge-phonon coupling dominates the Seebeck effect, which leads to a positive coefficient. This driving force drifts the majority carriers, electrons moving from the low-temperature surface to the high-temperature surface, developing a positive Seebeck coefficient. With higher electrical conductivities, the traditional entropy difference under a temperature difference dominates the Seebeck effect, which tends to be

negative for the n-type devices. This driving force diffuses electrons from the high-temperature surface to the low-temperature surface toward developing a negative Seebeck coefficient. Clearly, the major driving force of Seebeck effect can be tuned through adjusting surface polarization and entropy difference under a temperature difference. It should be noted that hopping mechanism dominates carrier transport in the organic composite PCBM:PMMA. As the PMMA composition is 30 wt% in the PCBM:PMMA composite, the hopping rate would increase and consequently boosts the charge mobility. This can essentially cause an increase on the electrical conductivity, as shown in Figure 3.2(b). Furthermore, increasing mobility can decrease the interaction time between charge and thermal vibration, weakening the charge-phonon coupling.[123,124] Consequently, this can decrease the driving force from temperature-dependent surface polarization in the development of Seebeck effect. Therefore, increasing the electrical conductivity can switch the Seebeck effect between polarization and entropy regimes.

Figure 3.3(a) shows the Seebeck effect from the device ITO/CN-MBE/Au with increasing temperature. The chemical structure of n-type CN-MBE is displayed in the inset of Figure 3.3(a). We can see that Seebeck coefficients are tuned from negative values to positive values with increasing temperature with the temperature cycle both from low to high and from high to low-temperatures. The change of the tunable Seebeck regimes is reversible. This Seebeck transition phenomenon can be repeated. At temperatures below 75 ^{o}C, Seebeck coefficients from n-type CN-MBE are negative. This can be attributed to electron diffusion from high- to low- temperature surface under the driving force of entropy difference. At temperatures above 75 ^{o}C, Seebeck coefficients change to positive values. This can be attributed to the driving force of temperature-dependent surface polarization from coupling of local polarization and thermal vibrations. With increasing temperature, the switch between negative and positive Seebeck coefficients for n-type CN-MBE directly confirms that the major driving force of the Seebeck effect can be tuned between temperature-dependent surface polarization and entropy difference, and this can come from the changeable electrical conductivity with the increasing temperature. It is because within the low temperature range, the charge mobility is higher compared with that within the high

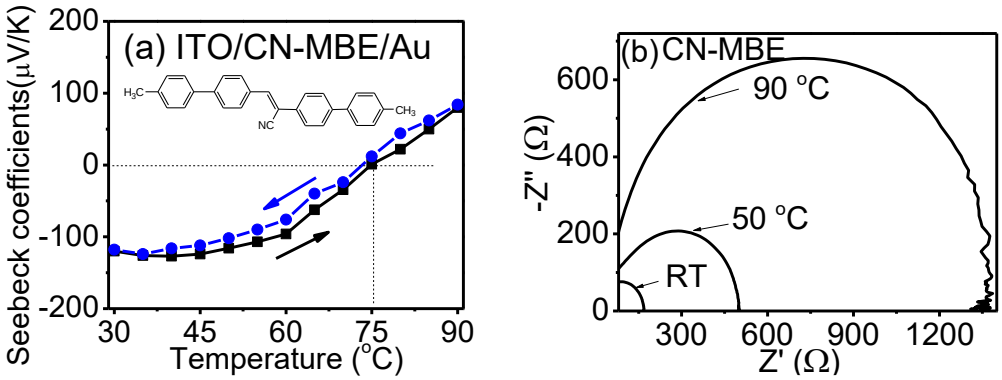

Figure 3.3 (a) Seebeck effect and (b) Cole-Cole characteristics for vertical thin-film devices based on the n-type organic semiconductor device: ITO/CN-MBE/Au.

temperature range due to the stronger phonon scattering at higher temperatures. The higher charge mobility indicates that the interaction time between charge and thermal vibration would be reduced. Thus, the charge-phonon coupling would be weakened. Therefore, the polarization effect from charge-phonon coupling would be decreased and the driving force of entropy difference would be enhanced in the low temperature range. So the Seebeck effect can be tuned between polarization and entropy regimes. Figure 3.3(b) shows the estimation of electrical conductivity of the devices at different temperatures by Cole-Cole characteristics. It can be seen that electrical conductivity of the devices decreases with increasing temperature, indicated by the increasing resistance Z (X=0) from the Cole-Cole curves. Therefore, the regime of the Seebeck coefficient from vertical thin-film devices can be tuned by adjusting electrical conductivities due to the competition of the two driving forces: the entropy difference and the temperature-dependent electrical polarization. The entropy difference drives diffusion of electrons from the high-temperature surface to the low-temperature surface for a negative Seebeck effect in n-type devices, while the temperature-dependent electrical polarization from the charge-phonon mechanism drives electrons from the low-temperature surface to the high-temperature surface, generating a positive Seebeck effect.

In our measurements we have removed the parameter of the built-in potential from the interface between CN-MBE/Au and CN-MBE/ITO in the determination of Seebeck voltage. Firstly, in dark condition under negligible temperature difference, the Seebeck voltage is ~0 μV/K based on ITO/CN-MBE/Au devices, while, under temperature difference, the Seebeck voltage is generated and the Seebeck coefficients are changed from negative values to positive values with increasing temperature. Secondly, to further confirm the phenomenon of the tunable Seebeck regimes, Au/CN-MBE/Au devices without the difference between work function of electrodes are studied (**Figure 3.4**), and the same tunable Seebeck regimes are obtained. The Seebeck coefficients are tuned from negative values to positive values with increasing temperature. Therefore, in this situation, in n-type ITO/CN-MBE/Au devices, the Seebeck coefficients can be changed from the entropy regime to the polarization regime with increasing temperature

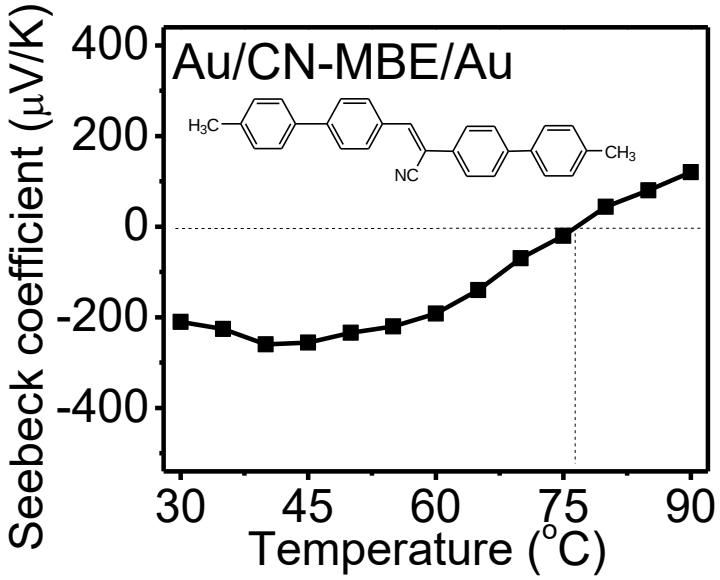

Figure 3.4 Seebeck coefficient of the n-type organic semiconductor device: Au/CN-MBE/Au.

due to the decreased electrical conductivity through the reduced charge mobility.

Now, we use the capacitance-frequency (C-f) measurements to explore the polarization regime from charge-phonon coupling at higher temperatures based on the n-type organic semiconductor device ITO/CN-MBE/Au. The capacitance-frequency (C-f) measurement were performed under dark condition by using dielectric spectrometer (Agilent E4980A LCR). In general, the capacitance-frequency characteristics can be divided into low and high-frequency regimes. The former and latter are associated with the electrode interface and bulk polarization behaviors, respectively. **Figure 3.5** shows the frequency-dependent capacitance characteristics at different temperatures. It should be noted that at high frequency the capacitance can essentially reflect the bulk polarization in thin films compared with the capacitance at low frequency. Here, we can see that at high frequency ($> 100\times10^3$ Hz) the capacitance increases with increasing temperature in the ITO/CN-MBE/Au device. This behavior indicates that increasing temperature can essentially lead to an increase in the bulk polarization in the CN-MBE film. With increasing bulk polarization we can expect that the charge transport experiences strong Coulombic interaction, leading to a decrease in carrier mobility at higher temperatures. The weaker charge mobility indicates that the interaction time between charge and thermal vibration would be enhanced. Thus, the charge-phonon coupling is enhanced at higher temperatures. The increase in the bulk polarization with increasing temperature reflects the strong coupling between local polarization and thermal vibration, which can directly develop the temperature-dependent polarization. Therefore, with increasing temperature the polarization effect ill increase while the driving force of entropy difference will decrease. Consequently, the Seebeck coefficient can be tuned between entropy and polarization regimes by the changing electrical conductivity due to the changeable charge mobility.

Figure 3.6 shows a schematic diagram for the development of the Seebeck effect in the vertical thin-film device: ITO/CN-MBE/Au. We can see that, on one hand, temperature-dependent surface polarization can establish a temperature-dependent built-in electrical field through coupling of local polarization and thermal vibration is developed between the high and low-temperature surface. The direction of the built-in electrical field is from the high-temperature to the low-temperature surface, as shown in the diagram. It drives the electrons from the low-temperature surface to the high-

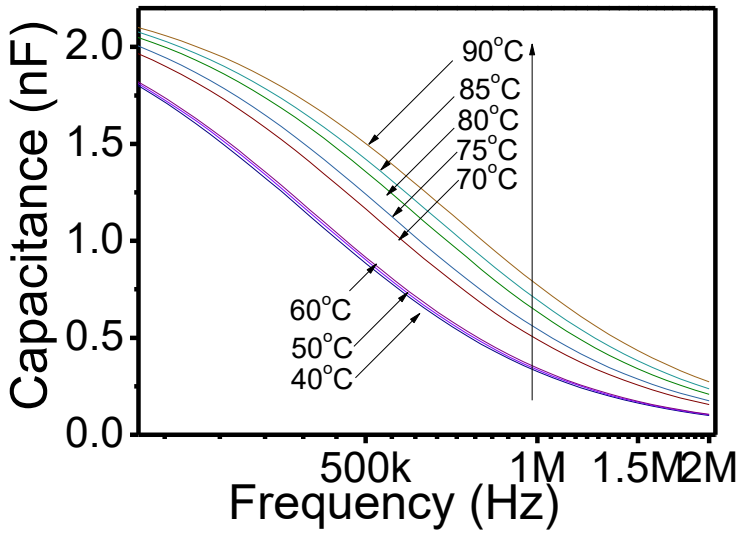

Figure 3.5 Capacitance-frequency (C-f) characteristics measured at different temperatures for ITO/CN-MBE/Au devices**.**

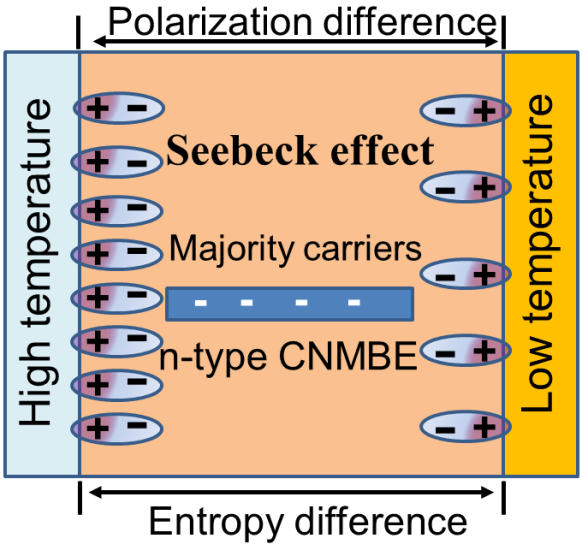

Figure 3.6 Schematic diagram to show charge diffusion towards development of the Seebeck effect under the driving forces of temperature-dependent electrical polarization and entropy difference in the vertical thin-film device: ITO/CN-MBE/Au. The average temperature difference detected between the high-temperature surface and the low-temperature surface is around 2.0 ^{o}C.

temperature surface and developing a positive Seebeck effect. On the other hand, the traditional driving force of entropy difference under a temperature difference can diffuse electrons from the high-temperature to the low-temperature surface toward developing a negative Seebeck effect. The competition of the two driving forces determine the sign of Seebeck coefficients. When the electrical conductivity is large at lower temperature in ITO/CN-MBE/Au devices, the traditional driving force of entropy difference dominates the process causing the device to show negative Seebeck coefficients. When the electrical conductivity is small at higher temperature in ITO/CN-MBE/Au devices, the driving force of temperature-dependent surface polarization dominates the process causing the device to show positive Seebeck coefficients. Consequently, the Seebeck effect from the vertical thin-film devices can be tuned between entropy difference and temperature-dependent surface polarization regimes controlled by changing the electrical conductivity.

3.4 Conclusion

In summary, we find that the Seebeck effect can be tuned between the entropy and polarization regimes by controlling electrical conductivity. Based on the vertical multi-layer thin-film electrode/n-type organic/electrode design, the Seebeck regimes are tuned by adjusting electrical conductivities via varying compositions of the films in ITO/PCBM:PMMA/Au devices and adjusting temperatures in ITO/CNMBE/Au devices. The ITO/PCBM:PMMA/Au device at 30 wt% PMMA and the ITO/CNMBE/Au device at lower temperatures exhibit higher electrical conductivities and generate negative Seebeck coefficients under the driving force of entropy difference. The ITO/PCBM:PMMA/Au device at 50 wt% PMMA and the ITO/CNMBE/Au device at higher temperatures exhibit lower electrical conductivities, and generate positive Seebeck coefficients due to the mechanism of polarization effect. Cleary, our experimental demonstration indicates that the Seebeck effect can be tuned between the entropy and polarization regimes by changing electrical conductivity.

Chapter 4

4 Solving conflicting problems in developing dual Seebeck and cooling effects in vertical organic thin-film devices

4.1 Introduction

Experimental studies have shown that attractive thermoelectric effects have been demonstrated based on thin-film structures and multi-component composites due to their high electrical conductivities but low thermal conductivities.[125-128] It should be pointed out that the two typical phenomena, Seebeck and cooling effects, have a conflicting requirement for the relationship between electrical and thermal conductivities. The cooling effect requires strong electron-phonon coupling for injected charge carriers to absorb the local heat from surface-thermal vibration.[129-131] On contrast, under the traditional driving force of entropy difference, the Seebeck effect requires a weak electron-phonon coupling to separate electrical and thermal conductivities.[132-135] Specifically, considering about the additional driving force of polarization, in the hybrid metal/active layer/metal thin-film device, the electron-phonon coupling can reflect as temperature-dependent surface-electrical polarization at each metal/organic interfaces. Consequently, low and high-temperature surfaces can inevitably exhibit low and high electrical polarizations, leading to an electrical field between two metal surfaces in the thin-film device. This electrical field provides a new mechanism to develop Seebeck effect by diffusing the charge carriers when a temperature difference is applied onto the thin-film devices. At the same time, the electron-phonon coupling presents a necessary condition for injected carriers to absorb heat from surface-thermal vibration for development of cooling effect. Therefore, using electron-phonon coupling indicates a possibility to solve the conflicting requirement to develop dual Seebeck and cooling effects from single metal/active layer/metal thin-film devices when temperature difference and electrical bias are applied separately. In this work, we will combine the electron-phonon coupling with the hybrid electrode/active

layer/electrode thin-film design to explore a solution of solving the conflicting requirement for developing dual Seebeck and cooling effects.

Thermionic cooling from single heterojunctions can have potential applications in thin-film devices. In general, the thermionic cooling can be realized by interfacial phonon absorption from injected charge carriers followed by the bulk transport of energetic carriers in thin-film devices under an external charge injection.[136-139] The thermionic injection forms an effective mechanism to absorb phonons and to generate energetic carriers in thin-film devices.[137-139] The transport of energetic carriers can then generate a cooling effect at the charge-injecting electrode. It should be noted that the oxide MoO_3 thin-films have been heavily used in organic electronic devices to enhance optoelectronic properties due to exceptional surface-semiconducting properties.[140-144] Therefore, the thermionic cooling effect developed from such oxide thin-film devices can have potential applications in organic electronics. The selected oxide MoO_3 has a high dielectric constant of ~ 40 at steady state.[145] From the high dielectric constant we can expect a large surface polarization on the MoO_3 film in the electrode/medium/electrode device under an electrical bias. As a consequence, the injected carriers can effectively absorb phonons through charge-phonon coupling mechanism at the electrode/oxide interface, generating a thermionic injection. It is noted that the charge-phonon coupling is a key parameter to determine the phonon absorption rate defined as the number of phonons absorbed at a given barrier. The charge-phonon coupling can be realized in a medium when a charge electrically polarizes the surrounding lattice. The electrical interaction between a charge and polarized surrounding lattice can essentially determine the charge-phonon coupling strength. We should further note that the surfaces can exhibit stronger charge-phonon coupling as compared to the bulk in thin films due to un-balanced polarizations. In particular, increasing the surface polarization can enhance the interfacial charge-phonon coupling in thin films. With the charge-phonon coupling, the injected carriers can absorb the surface phonons to realize thermionic injection under an electrical bias, generating thermionic cooling effect. In this work, we explore the cooling effect by using electrically polarizable interface based on high-dielectric oxide MoO_3 based on

single heterojunction devices with the architecture of electrode/medium/electrode. Here we observe that the single-heterojunction ITO/MoO_3/Au device can generate a clear cooling phenomenon (0.10 ºC) under an extremely low injection current of 0.50 mA/cm^2. Our analysis indicates that the thermionic cooling effect is controlled by phonon absorption from injected charge carriers, Joule heating from charge transport, and heat transfer in the organic thin-film electrode/medium/electrode devices. Furthermore, we find that this cooling effect can be largely enhanced by a factor of 2 when a ferroelectric polymer [P(VDF-TrFE)] film is used in the Au/P(VDF-TrEE)/MoO_3/ITO device. This experimental finding presents promising possibilities of enhancing thermionic cooling by using electrically-polarizable surface in organic single-heterojunction devices.[120]

4.2 Experimental

The thin-film devices were fabricated with the sandwich Au/medium/ITO structure based on the following procedures. The MoO_3 layer with different thickness, 30 nm, 40 nm and 60 nm, was respectively evaporated onto the pre-cleaned ITO electrodes followed by a 50 nm thick gold deposition under the vacuum of $4x10^{-6}$ Torr. To introduce a ferroelectric interface, 10 nm, 20 nm and 40 nm thick P(VDF-TrFE) layers were respectively obtained by spin-casting from acetone solution onto the 30 nm MoO_3 thin film under nitrogen atmosphere to fabricate the Au/P(VDF-TrFE)/MoO_3/ITO device. The single P(VDF-TrFE) layer was obtained by spin-casting onto the pre-cleaned ITO electrodes to fabricate the Au/P(VDF-TrFE)/ITO device. The fabricated devices were then heated at 135 ºC for 20 min to improve the device quality. The active area of the devices is 0.1 cm^2. The P(VDF-TrFE) was purchased from Measure Specialties, and Polymethylmethacrylate (PMMA) and MoO_3 were purchased from Sigma-Aldrich. By following standard procedures to measure the thermionic cooling effect, the top gold (Au) surface and the bottom ITO surface are used as charge-injecting and charge-collecting electrodes, respectively. The two K-type thermocouples were attached to the glass substrate (underneath the ITO electrode) and

the Au electrode to measure the cooling effect in the Au/MoO_3/ITO, Au/P(VDF-TrFE)/MoO_3/ITO, & Au/P(VDF-TrFE)/ITO devices. In this design, the temperature on glass substrate provides a reference temperature while the cooling temperature was developed and measured on the Au electrode surface. In order to accurately measure the cooling temperature, the thermocouple on the Au electrode was attached by using the following method to avoid the possible electrical interference horizontally on the Au electrode plane: a 5 nm thick PMMA layer is used to electrically separate the Au and thermocouples. The charge (hole) injection was realized from the positive Au electrode. The electrical current was controlled by a Keithley 2400 power supply. The temperatures on ITO and Au surfaces were measured using an InstruNet Model 100 Input/Output System. Each temperature point was measured five minutes after the electrical bias was applied. The integration time of recording each temperature was about 0.004 seconds. The temperature errors are less than 0.03 ºC. The ferroelectric properties of the P(VDF-TrFE) film (thickness 250 nm) were characterized by using Precision Materials Analyzer, purchased from Radiant Technology, INC. The current-voltage (*I-V*) measurements were performed by using Lab Tracer software along with a Keithley 2400 power supply. The Cole-Cole characteristics were characterized by using an impedance spectrometer (Agilent, E4980A), and the bias used for the measurement is zero.

4.3 Results and Discussions

Figure 4.1(a) & (b) schematically summarizes thermionic cooling effect developed by single heterojunctions without and with ferroelectric surface, Au/MoO_3/ITO & Au/P(VDF-TrFE)/MoO_3/ITO, respectively. The device structure based on Au/MoO_3/ITO to show charge injection direction and temperature measurements is presented in **Figure 4.1(c)**. For the Au/P(VDF-TrFE)/MoO_3/ITO device, the P(VDF-TrFE) layer is inserted between MoO_3 and the top Au electrode. Essentially, the cooling effect is obtained from the charge-injecting Au electrode when the holes are injected into the high-dielectric MoO_3 film through the ferroelectric P(VDF-TrFE) layer based

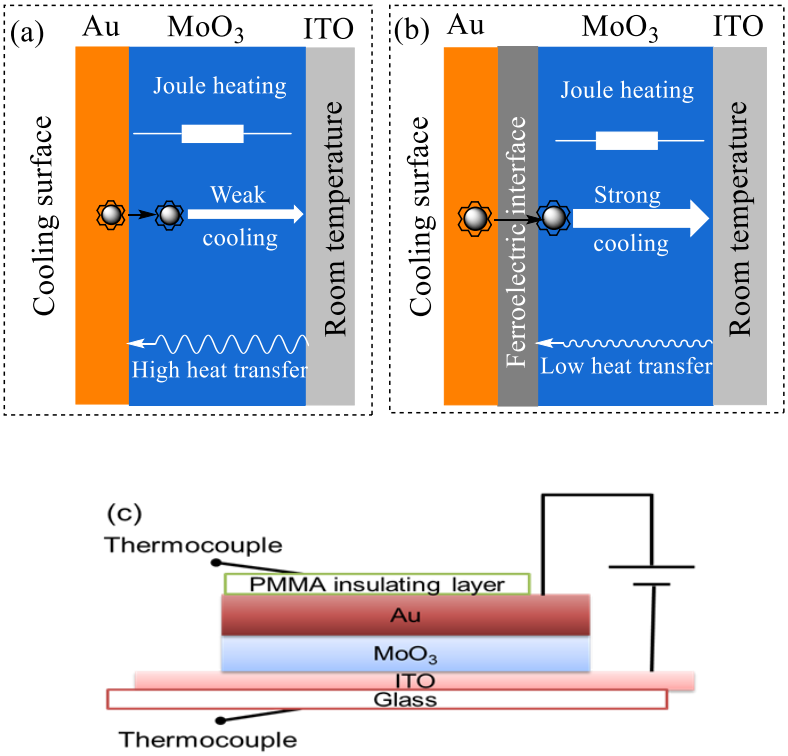

Figure 4.1 Band diagrams and device structure to show thermionic cooling developed by three competing processes: (i) phonon absorption from injected carriers, (ii) Joule heating from transport of injected carriers, and (iii) heat transfer through phonon conduction. The solid sphere circled with waves represents injected hole coupled with phonons through thermionic process. The phonon absorption is essentially realized when the holes are injected through thermionic process based on charge-phonon coupling. (a): Au/MoO_3/ITO device. (b): Au/P(VDF-TrFE)/MoO_3/ITO device. (c): Device structure with temperature measurements and charge injection.

on thermionic process and followed by the charge transport to the charge-collecting ITO electrode through the MoO_3 film. The thermionic cooling effect is determined by the following three competing processes. Firstly, the phonon absorption must be realized by the injected holes through the interaction between the charge carriers on injecting electrode and the surface polarization of medium layer in the thin-film electrode/medium/electrode devices. Secondly, the transport of injected carriers can generate a Joule heating which can decrease the cooling effect developed by the phonon absorption from injected carriers. Thirdly, the temperature difference between the two electrodes can generate a heat transfer, leading to a reduction on the cooling effect. Here, we demonstrate a thermionic cooling effect (0.10 °C) in single-heterojunction Au/MoO_3/ITO devices by controlling these three competing processes through changing medium thickness and injection current. Furthermore, we find that introducing ferroelectric P(VDF-TrFE) interface can largely enhance the thermionic cooling effect (from 0.10 °C to 0.20 °C) by decreasing the thermal transfer but still allowing charge injection in the Au/P(VDF-TrFE)/MoO_3/ITO device.

In our work, the cooling effect occurs on the hole-injecting electrode Au electrode surface in the Au/MoO_3/ITO device. We can see in **Figure 4.2**(a) and (b) that the temperature on the charge-injecting electrode Au surface gradually decreases, while the temperature on the charge-collecting electrode ITO surface slightly increases, as the injection current is increased. This experimental phenomenon clearly suggests a cooling effect occurring on the charge-injecting Au surface in the Au/MoO_3/ITO device. With increasing electrical injection currents, the cooling effect first increases and then decreases in the Au/MoO_3/ITO devices. For the device with the 30 nm MoO_3 layer, the maximal cooling of 0.10 ºC is observed at the injection current of 0.50 mA/cm^2. For the device with the 40 nm MoO_3 layer, the best cooling of 0.07 ºC is observed at the injection current of 0.70 mA/cm^2. No cooling effect is observed in the device with the 60 nm MoO_3 layer (Figure 4.2(c)). Here, we can see that the cooling effect is a thickness-dependent phenomenon in the Au/MoO_3/ITO devices. Increasing the MoO_3 thickness leads to a decrease on the cooling effect. Nevertheless, the observed thermionic cooling effect suggests that the injected charge carriers can absorb phonons

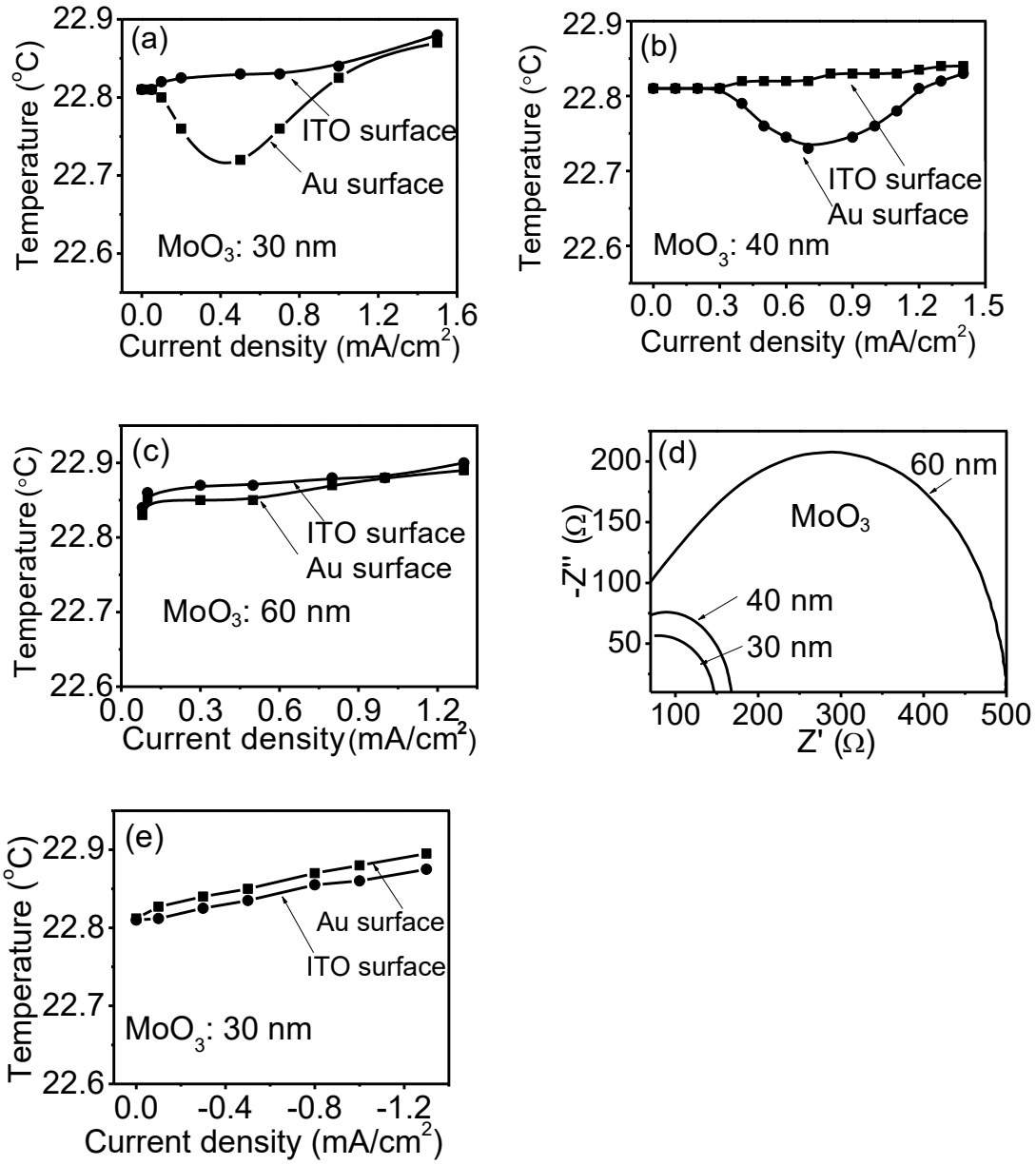

Figure 4.2 Cooling effect at different current densities. (a): Au/MoO_3 (30nm)/ITO; (b): Au/MoO_3 (40nm)/ITO; (c): Au/MoO_3 (60nm)/ITO. The Au and ITO serve as charge-injecting and collecting electrodes, respectively. The temperature error is ~ 0.03 ºC. (d): Cole-Cole characteristics to show different resistances for Au/MoO_3/ITO devices with the different MoO_3 thicknesses. (e): Reverse bias effects on cooling in Au/MoO_3(30nm)/ITO device.

through thermionic injection at the Au/MoO_3 interface through electron-phonon coupling mechanism. It should be noted that increasing the MoO_3 film thickness can increase the bulk resistance, which can in principle increase the Joule heating and decreases the thermionic cooling effect. Figure 4.2(d) shows the Cole-Cole characteristics measured from 20 HZ to 2 MHZ for the device with different MoO_3 film thicknesses. The Cole-Cole equation is generally given by

$$Z = R + iX \quad (1)$$

The value generated by the Cole equation is a complex value *Z* containing the real part, resistance *R*, and the imaginary part, reactance *X*. The *R* could include both bulk resistance and interface-contact resistance.[146-148] Here, we use the *R* value at *X*=0 to reflect the device resistance. Based on the Cole-Cole characteristics, we can see in Figure 4.2(d) that increasing MoO_3 film thickness from 30 nm to 40 nm and 60 nm can indeed cause an increase on the resistance from 147 Ω to 168 Ω and 500 Ω in the Au/MoO_3/ITO devices. In general, the evaporated Au atoms can have penetration into the underlying layer during thermal evaporation. Therefore, the MoO_3 layer can be divided into doped and undoped zones in the MoO_3 layer upon Au deposition. Changing the MoO_3 layer thickness can change the thickness ratio between the doped and undoped zones. This can largely change the device resistance when varying the MoO_3 layer thickness, as shown by the Cole-Cole results in Figure 4.2(d). Changing the device resistance can then modify the Joule heating. Clearly, the thickness-dependent cooling phenomenon indicates that the Joule heating is involved in the development of cooling effect. On the other hand, we should note that the slight increase of ITO surface temperature can be attributed to the simultaneous actions of Joule heating and thermal transfer between the two electrode surfaces in the Au/MoO_3/ITO devices. In addition, when a reverse bias is applied in the situation where the ITO and Au are used as charge-injecting and charge-collecting electrodes, a heating effect can be observed on the Au electrode surface due to the Joule heating (Figure 4.2(e)). This result indicates that the ITO surface does not provide a thermionic injection and consequently the Joule heating becomes a dominant phenomenon. This further supports the thermionic cooling mechanism.

In the thin-film Au/MoO_3/ITO device when the Au and ITO electrodes respectively served as charge-injecting and collecting electrodes, the injected holes are essentially responsible for absorbing phonons through electron-phonon coupling mechanism to overcome the potential barrier at the Au/MoO_3 interface. In general, the thermionic cooling effect is the outcome from three simultaneous processes: phonon absorption from injected holes, Joule heating due to electrical transport, and heat transfer between the higher-temperature ITO and the lower-temperature Au through phonon conduction, in the Au/MoO_3/ITO thin-film device. To understand these three simultaneous processes, we discuss the effects of the injection current density on the cooling phenomenon. In principle, adjusting the injection current density can change the competition between phonon absorption, Joule heating, and heat transfer, and consequently lead to an optimization on the cooling effect. We can see in Figure 4.2(a) & (b) that the maximal cooling is realized at the different critical currents of 0.50 mA/cm^2 and 0.70 mA/cm^2 in the 30 nm and 40 nm thick MoO_3 devices, respectively. Increasing the injection current towards the critical current density causes an increase on cooling effect, leading to an increasing cooling zone. In this increasing cooling zone, the phonon absorption through thermionic injection plays a primary role upon increasing the injection current. The Joule heating and heat transfer become secondary phenomena with increasing injection currents. However, further increasing the injection current beyond the critical current density causes a decrease on cooling effect, generating a decreasing cooling zone. In this decreasing cooling zone, the Joule heating and thermal transfer becomes primary phenomena with increasing the injection current. We should also note that increasing the MoO_3 film thickness can increase the bulk resistance and consequently the Joule heating. This can decrease the thermionic cooling effect. As indicated in Figure 4.2(c), when the MoO_3 thickness is increased to 60 nm, no obvious cooling effect can be obtained. Nevertheless, the cooling dependence on injection currents at different MoO_3 film thicknesses can confirm that the three processes: phonon absorption from injected charge carriers, Joule heating from electrical transport, and heat transfer from thermal conduction are all together responsible for developing the cooling effect in single-heterojunction devices.

Now we discuss ferroelectric surface effects on the cooling effect by using electrically-polarizable polymer [P(VDF-TrFE)] thin film. The P(VDF-TrFE) layer can exhibit typical ferroelectric properties with strong surface polarization in response to an external electric field. The ferroelectric properties are shown in **Figure 4.3(a)** for the Au/P(VDF-TrEE)/ITO device. The displaced polarization density is presented as a function of applied electric bias, and the ferroelectric hysteresis loop is obtained. With this ferroelectric property we can expect that an applied electric bias can induce strong surface polarization on the P(VDF-TrEE) film. Here, the ferroelectric surface provides two basic functions: (i) reducing the heat transfer between anode and cathode due to its low thermal conductivity (~0.1 W/m/K)[149,150] and (ii) allowing injection current through polarization-assisted process in the thin-film design. Firstly, we can show that the ferroelectric polarization can allow thermionic injection through the P(VDF-TrFE) layer. It can be seen in **Figure 4.3(b)** that the injection current generates a weak cooling phenomenon in the single layer P(VDF-TrFE) (30 nm) device. The maximal cooling of 0.06 ^{o}C is realized at the critical current of 0.04 mA/cm^2. The current-voltage (I-V) characteristics indicates that the injection current can indeed occur for generating the cooling effect in the Au/P(VDF-TrFE)/ITO device (**Figure 4.3(c)**). On contrast, non-electrically polarizable polymer films such as PMMA give negligible cooling effect in our thin-film electrode/medium/electrode devices due to insufficient injection current. Here, the P(VDF-TrFE) has dual heat insulating and ferroelectric properties.[151-156] The ferroelectric polarization can lead to a strong surface polarization on the P(VDF-TrFE) film in the Au/P(VDF-TrFE)/ITO device under an electrical bias. It should be noted that the P(VDF-TrFE) film thickness used in our cooling devices is around 30 nm, much thinner than that for the measurement of hysteresis characteristics. With a thinner ferroelectric film a relatively low bias can still establish a strong electrical field to induce the surface polarization in the P(VDF-TrFE)-based cooling devices. Based on the observed cooling effect (Figure 4.3(b)), we can suggest that the surface polarization can still allow certain thermionic injection through electron-phonon coupling mechanism, generating a cooling effect in the Au/P(VDF-TrFE)/ITO device. Therefore, the P(VDF-TrFE) thin films can be used as a unique material to further enhance the

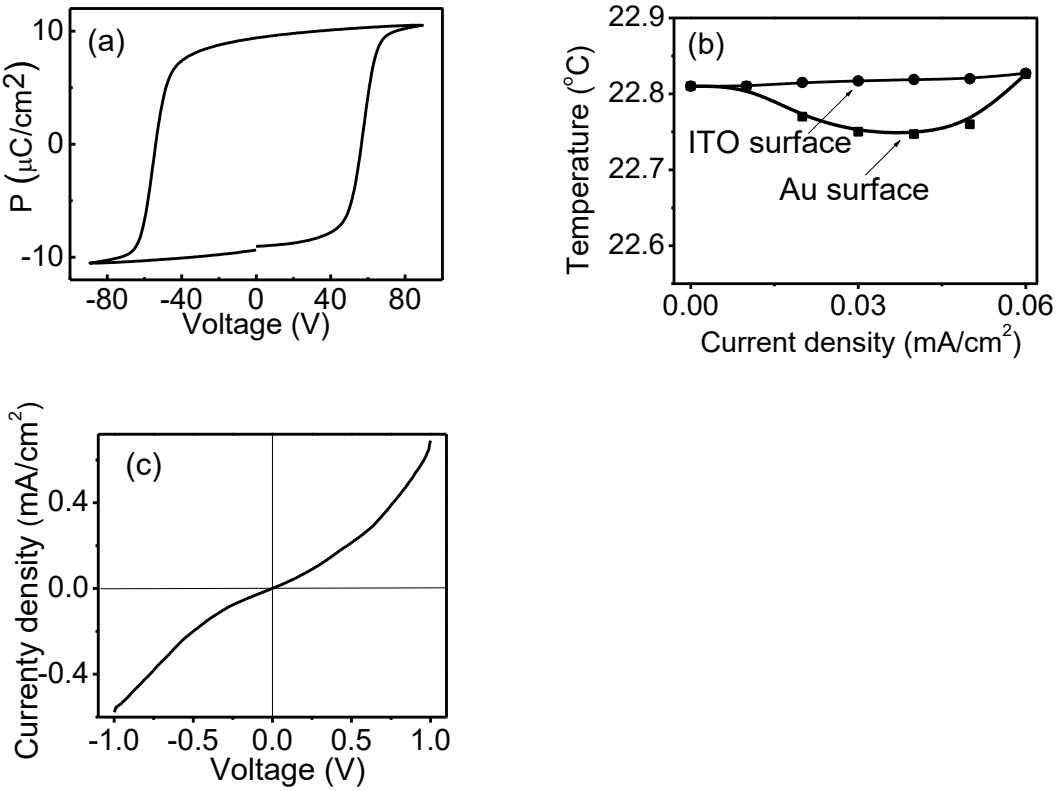

Figure 4.3 (a) Ferroelectric characteristics from Au/P(VDF-TrEE)/ITO device and the P(VDF-TrEE) film thickness is 250 nm. Cooling effect and I-V characteristics for Au/P(VDF-TrFE)/ITO device with P(VDF-TrFE) film thickness around 30 nm. (b): Cooling effect at different current densities; (c): I-V characteristics.

cooling effect in single-heterojunction devices based on its low thermal conductivity and allowed charge injection.

Now we discuss the effects of ferroelectric surface on thermionic cooling phenomenon. **Figure 4.4** shows the cooling phenomenon at different injection currents from the Au/P(VDF-TrFE)/MoO_3/ITO devices with three different P(VDF-TrFE) thicknesses (10nm, 20 nm, & 40nm). The device with the 10 nm P(VDF-TrFE) layer gives the maximal cooling of 0.20 ºC at the injection current of 0.15 mA/cm^2 (Figure 4.4(a)). By comparing the cooling from single-layer Au/MoO_3/ITO and double-layer Au/P(VDF-TrFE)/MoO_3/ITO devices (Figure 4.2(a) and Figure 4.4(a)), we can see that using electrically-polarizable P(VDF-TrFE) layer can largely enhance the cooling effect by a factor of 2. It should be noted that inorganic single heterostructures can show much larger thermionic cooling phenomena (2.8 ºC) at higher injection currents (> 5000 mA/cm^2). Here, we show that an extremely low current injection of 0.15 mA/cm^2 can generate an appreciable thermionic cooling of 0.20 ºC in the Au/P(VDF-TrFE)/MoO_3/ITO device. Our intention is to discuss the ferroelectric interface effects on thermionic cooling phenomena based on thin-film electrode/medium/electrode design.

We should note that a thicker P(VDF-TrFE) layer (20 nm) leads to a much smaller cooling (0.09 ºC) at a relatively higher injection current of 0.31 mA/cm^2, as compared to a thinner P(VDF-TrFE) layer (10 nm) with the cooling of 0.20 °C at 0.15 mA/cm^2 in the Au/P(VDF-TrFE)/MoO_3/ITO device (Figure 4.4(b)). The 40 nm P(VDF-TrFE) layer only generates very weak cooling effect (Figure 4.4(c)). Theoretically, increasing the P(VDF-TrFE) thickness can weaken the interaction between the injected charge carriers and the surface polarization on MoO_3 film, and consequently weakens the electron-phonon interaction required for thermionic injection. On the other hand, the P(VDF-TrFE) layer can decrease the heat transfer between charge-injecting and collecting electrodes due to its low thermal conductivity. Obviously, the P(VDF-TrFE) layer can generate two opposite contributions to the cooling effect: decreasing the thermal transfer between two electrodes, which enhances the cooling effect, and weakening the electron-phonon interaction for injecting charge carriers, which is

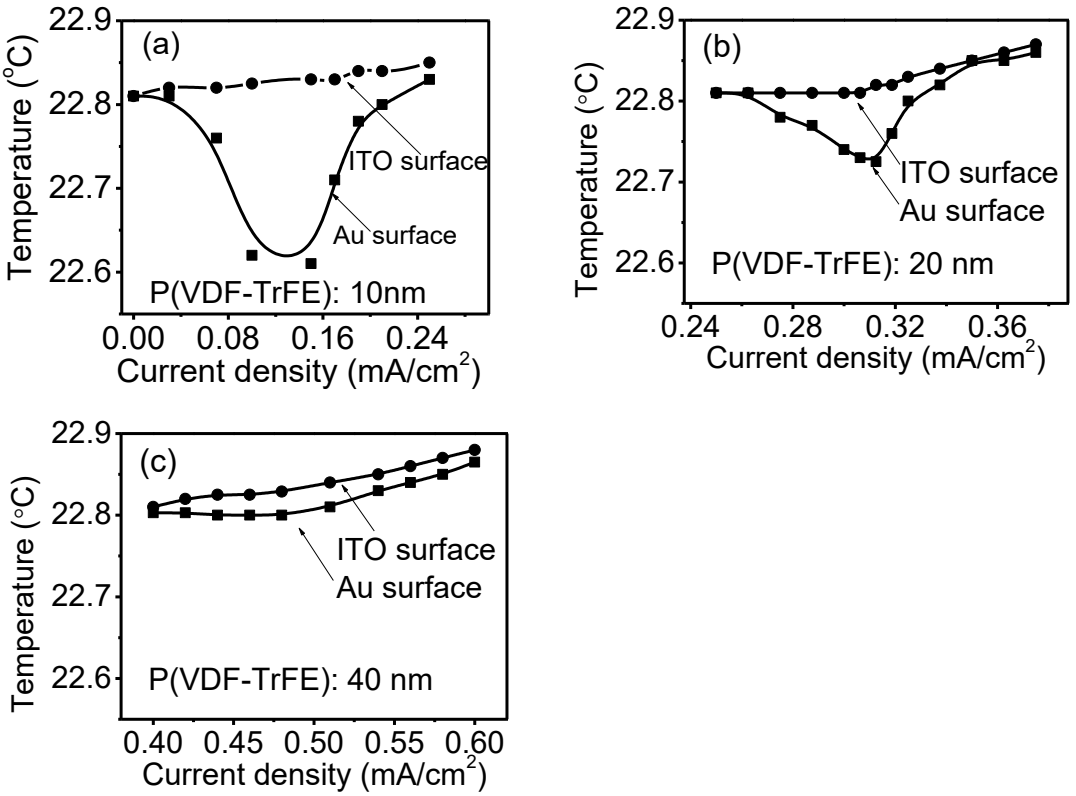

Figure 4.4 Cooling effect at different current densities from Au/P(VDF-TrFE)/MoO_3/ITO devices with different P(VDF-TrFE) thicknesses. (a): P(VDF-TrFE) = 10 nm, (b): P(VDF-TrFE) = 20 nm, (c): P(VDF-TrFE) = 40 nm. The MoO_3 layer thickness is fixed at 30 nm. The Au and ITO serve as charge-injecting and collecting electrodes. The temperature error is ~ 0.03 ºC. The solid dots and squares are experimental data for temperatures on ITO and Au surfaces. The solid lines are eye-guided curves to show cooling effect.

detrimental to the cooling effect. Adjusting the P(VDF-TrFE) thickness can then change these two opposite contributions. With a thinner P(VDF-TrFE) (10 nm) layer, the reduction on thermal transfer becomes primary component, leading to an enhanced cooling. However, with a thicker P(VDF-TrFE) layer, the reduction on the interaction between the injected charge carriers and the surface polarization becomes a major component, decreasing the cooling effect. Clearly, the P(VDF-TrFE) thickness-dependent cooling results provide further evidence that the observed cooling effect is generated under electron-phonon coupling mechanism through thermionic injection in our single-heterojunction devices.

Now we further confirm that the observed cooling is a thermionic phenomenon induced by injection current by repeating measurement cycles. **Figure 4.5** displays the cooling effect in different measurement cycles as a function of time for the Au/P(VDF-TrFE)/MoO_3/ITO thin-film device. At the constant current of 0.10 mA/cm^2, we can see that the temperature on charge-injecting Au electrode decreases from room temperature (22.81 ºC) to 22.62 ºC. After the injection current is ceased, the temperature on the Au electrode gradually increases towards room temperature due to thermal dissipation. When the electrical current (0.15 mA/cm^2) is re-applied, the temperature on Au electrode decreases again to generate a cooling effect. This reproducible experimental observation confirms that the cooling phenomenon is indeed a thermionic cooling phenomenon generated by the injection current in the Au/P(VDF-TrFE)/MoO_3/ITO thin-film device.

The thermionic injection is a key component in developing the cooling phenomena in our thin-film devices. In general, a thermionic injection can significantly occur at a low potential barrier at electrode/medium interface through charge-phonon coupling mechanism. In the Au/MoO_3/ITO device, the Au/MoO_3 interface forms a substantial potential barrier for the injected holes, according to the workfunction of injecting (Au) electrode and the energy levels of MoO_3.[143,157,158] However, the Au/MoO_3 interface can normally exhibit a large density of defects caused by thin-film formation and electrode deposition, leading to a significant band bending.[140,157] In this situation, a thermionic injection can occur to absorb local phonons for realizing thermionic cooling even though the potential barrier is much larger than thermal energies. It can be seen in

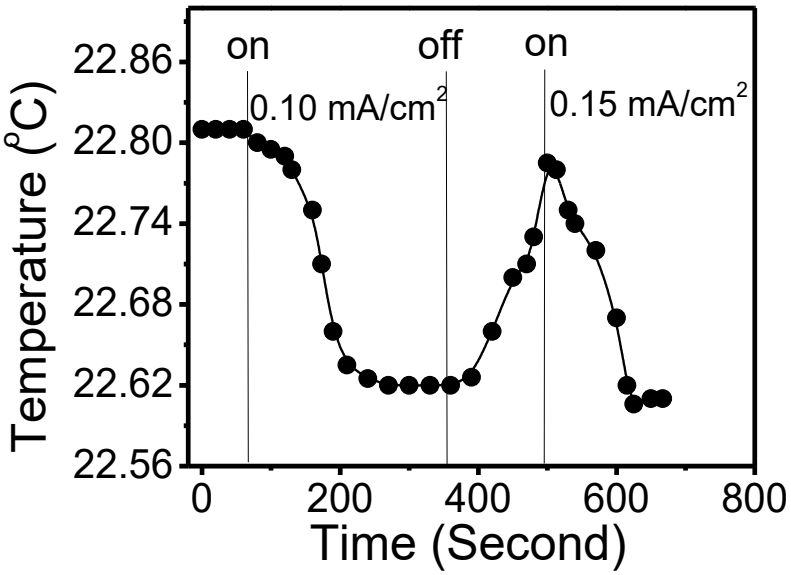

Figure 4.5 Cooling effect is developed as a function of time at constant injection currents in Au/P(VDF-TrFE)/MoO_3/ITO device. The P(VDF-TrFE) and MoO_3 are 10 nm and 30 nm in thickness, respectively.

Figure 4.6 that our thin-film devices show both positive and negative *I-V* characteristics with low turn-on voltages. The low turn-on voltages suggest that thermionic injection is activated to generate thermionic cooling in the Au/MoO_3/ITO and Au/P(VDF-TrFE)/MoO_3/ITO devices. Thermionic injection requires multi-phonon absorption to overcome interfacial barriers. In general, the charge injection at an interfacial barrier can undergo tunneling and thermionic processes.[159-164] The former and latter can coexist in a charge injection in thin-film devices.[165,166] However, tunneling and thermionic injection can become dominant processes at high and low barriers, respectively. In particular, a thermionic injection can significantly occur at a low potential barrier at electrode/medium interface through charge-phonon coupling mechanism.

Figure 4.7 shows Seebeck coefficients generated from the Au/P(VDF-TrFE)/MoO_3/ITO device. We can see that the Seebeck coefficients exceeds 1100 μV/K at 60 ^oC under the additional driving force of temperature-dependent surface polarization. Therefore, by combining organic ferroelectric polymer (P(VDF-TrFE)) with high-dielectric MoO_3, we have successfully developed both high Seebeck (1100μV/K at 60ºC) and cooling (0.26 ºC at a very low current injection of 0.15 mA/cm^2) effects from a single thin-film Au/P(VDF-TrFE)/MoO_3/ITO device when a temperature difference and an electrical injection are applied separately. The dual Seebeck and cooling effects, observed from the single inorganic/organic thin-film device, indicate that the electron-phonon coupling through hybrid organic/inorganic thin-film design can become a new mechanism to develop Seebeck and cooling effects with co-operative relationship.

Figure 4.8 show the *C-V* characteristics for Au/P(VDF-TrFE)/MoO_3/ITO devices at different temperatures under dark condition. We can see that the device shows a bias-dependent capacitance in dark condition, thus indicating field-dependent surface polarization. In particular, the capacitance for the device increases with increasing temperature. This experimental observation provides an evidence that the temperature-dependent surface polarization exists in the Au/P(VDF-TrFE)/MoO_3/ITO devices. Furthermore, the greatly increased capacitance at zero bias with increasing temperature, 6.2 nF at room temperature and 13.8 nF at 130 ^oC for the zero-bias capacitance, which

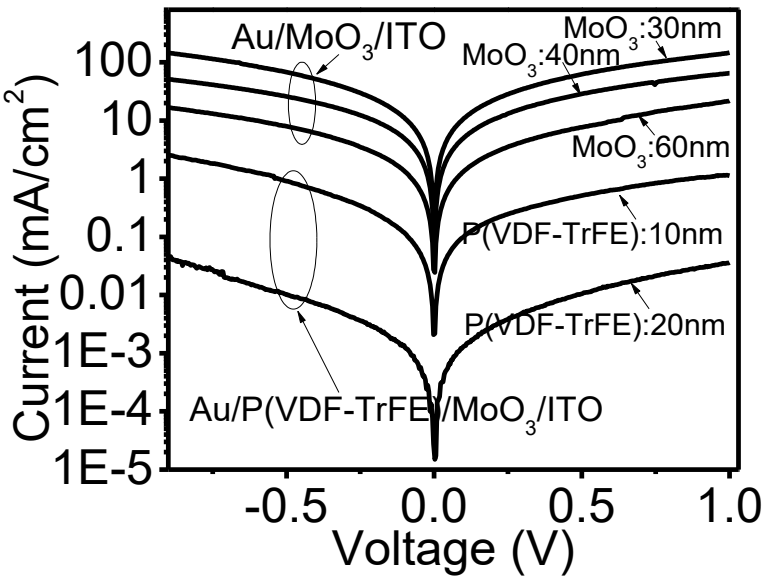

Figure 4.6 I-V characteristics for Au/MoO_3/ITO and Au/P(VDF-TrFE)/MoO_3/ITO devices. The MoO_3 was set at 30 nm, 40 nm, and 60 nm in Au/MoO_3/ITO device. The P(VDF-TrFE) thickness was set at 10 nm and 20 nm with fixed MoO_3 thickness of 30 nm in Au/P(VDF-TrFE)/MoO_3/ITO device.

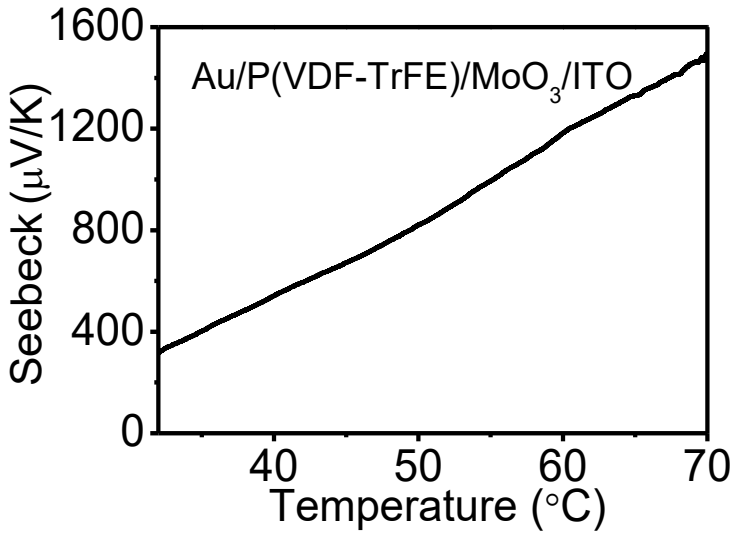

Figure 4.7 Seebeck effect for the hybrid thin-film device: Au/P(VDF-TrFE)/MoO_3/ ITO. The P(VDF-TrFE) and MoO_3 are 10 nm and 30 nm in thickness, respectively. Temperature difference is around 1.2 ^oC

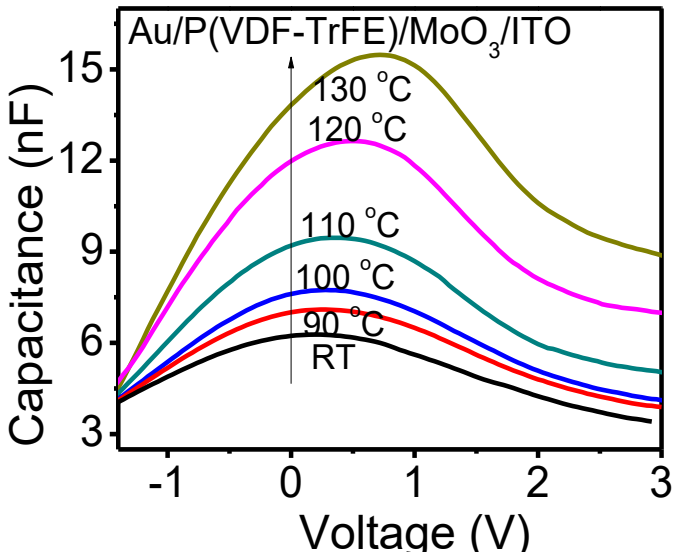

Figure 4.8 Capacitance-voltage (C-V) characteristics at different temperatures for the thermoelectric device Au/P(VDF-TrFE)/MoO_3/ITO.

increases by a factor of 2.2, confirms that the Au/P(VDF-TrFE)/MoO_3/ITO design can generate strong temperature-dependent surface polarization and consequently provide a strong driving force, in addition to entropy difference, to develop Seebeck effects in the vertical metal/polymer/metal thin-film devices.

4.4 Conclusion

In this chapter, by combining organic ferroelectric polymer (P(VDF-TrFE)) with high-dielectric MoO_3, we have developed high Seebeck effect and cooling effect at a very low current injection from a single organic/inorganic thin-film Au/P(VDF-TrFE)/MoO_3/ITO device when a temperature difference and an electrical injection are applied separately. Using the electron-phonon coupling through hybrid organic/inorganic thin-film design can cooperatively develop the Seebeck and cooling effects in organic thermoelectrics. We explored the effects of ferroelectric surface on thermionic cooling in single-heterojunction devices with thin-film electrode/medium/electrode design based on high-dielectric MoO_3 oxide and ferroelectric polymer P(VDF-TrFE). Firstly, we observed that the single-heterojunction Au/MoO_3/ITO device can generate a cooling phenomenon of 0.10 °C at a low injection of current of 0.50 mA/cm^2. From the current-dependent and thickness-dependent cooling results we can suggest that the thermionic cooling effect is generated by three competing processes: (i) phonon absorption from thermionic injection at electrode/medium interface, (ii) Joule heating from the transport of injected carriers, and (iii) heat transfer between charge-injecting and charge-collecting electrodes. Furthermore, we find that inserting a ferroelectric P(VDF-TrFE) interface can largely enhance the cooling effect from 0.10 °C to 0.20 ºC by 2 folds in the Au/P(VDF-TrFE)/MoO_3/ITO device. This experimental finding suggests that a ferroelectric interface can decrease the thermal transfer due to its low thermal conductivity but still allows a thermionic injection due to its ferroelectric polarization to enhance the thermionic cooling effect in the Au/P(VDF-TrFE)/MoO_3/ITO device. Therefore, using

high-dielectric layer and ferroelectric interface presents a promising approach to generate the cooling effect based on single-heterojunction thin-film devices.

Moreover, by combining organic ferroelectric polymer (P(VDF-TrFE)) with high-dielectric MoO_3, we have developed both high Seebeck effect, 1100μV/K at 60ºC, and cooling effect, 0.26 ºC at a very low current injection of 0.15 mA/cm^2, from a single organic/inorganic thin-film Au/P(VDF-TrFE)/MoO_3/ITO device when a temperature difference and an electrical injection are applied separately. Using the electron-phonon coupling through hybrid organic/inorganic thin-film design can present a novel method to cooperatively develop the Seebeck and cooling effects in organic thermoelectrics.

Chapter 5

5 Using Seebeck effects to study n and p-type properties in organo-metal halide perovskites

5.1 Introduction

Organo-metal halide perovskites have become interesting multifunctional materials with high-efficiency photovoltaic response, [167 - 169] largely tunable electroluminescence, [170 - 172] low-threshold lasing actions, [173, 174] and magneto-optic properties.[175,176] In general, the organic-inorganic perovskites can be prepared with single-halide or mixed-halide structures with co-existed electrical polarizations and semiconducting properties respectively from organic and inorganic components.[177-179] The experimental studies have shown that the single-halide and mixed halide perovskites can exhibit largely different properties in charge transport and excited states in photovoltaic, [180, 181] light-emitting,[171,173] and lasing applications[173] due to their different properties in transport and excited states. In this work we explore p-type and n-type semiconducting properties from single and mixed halide perovskites (called $CH_3NH_3PbI_3$ and $CH_3NH_3PbI_xCl_{3-x}$ hereafter) by using Seebeck effects. In principle, the n-type and p-type perovskites can exhibit distinctive behaviors in both charge transport and excited states due to different majority carriers.[182-184] Here, we vary the composition between organic and inorganic components to change the electrical polarizations and semiconducting properties in the organic-inorganic halide perovskites. We find that the n-type and p-type properties in organo-metal halide perovskites can be gradually switched when the organic and inorganic compositions are varied between $CH_3NH_3PbI_3$ and $CH_3NH_3PbI_xCl_{3-x}$ perovskites based on the lateral Seebeck measurements. In principle, the Seebeck effects can be measured in two different ways by applying a temperature gradient vertically or laterally to film-plane direction, namely vertical and lateral Seebeck measurements. In our early studies we have found that the Seebeck measurements based on the vertical multi-layer device provide an opportunity to explore an additional driving force to diffuse majority carriers between high and low temperature surfaces, based on temperature-dependent surface polarization, for developing Seebeck effects. However, the sign of Seebeck coefficient becomes ambiguous to determine the majority carriers in the Seebeck measurements

based on vertical thin film devices. In this work, we use the lateral Seebeck measurements as an un-ambiguous method to determine the n-type or p-type semiconducting properties. With this lateral design the Seebeck effects are essentially developed by the diffusion of majority carriers driven by the entropy difference between high and low-temperature contacts. Therefore, measuring the Seebeck coefficients can indicate the n-type and p-type properties in the organic-inorganic halide perovskites while the electrical polarizations and semiconducting properties are changed by varying the organic/inorganic compositions.

5.2 Experimental

Figure 5.1 shows the device structure to measure Seebeck effects with a lateral Au-perovskite-Au geometry. The perovskite film has the thickness of around 200 nm with the length of 2 mm between the two Au film contacts. Specifically, according to the publications, the organo-metal halide perovskite precursors were prepared by mixing Methylammonium iodide (MAI) separately with lead chloride ($PbCl_2$) and lead iodide (PbI_2) in anhydrous dimethylformamide (DMF). The single halide perovskites ($CH_3NH_3PbI_3$) were prepared by mixing MAI and PbI_2 with the molar ratio of 1:1. The mixed halide perovskites ($CH_3NH_3PbI_{3-x}Cl_x$) were prepared by mixing MAI and $PbCl_2$ with the molar ratio of 3:1. The single and mixed halide perovskite precursors were then stirred for 12 hours at 60℃ and followed by filtration (0.45μm PVDF filters). The $CH_3NH_3PbI_3$ and $CH_3NH_3PbI_{3-x}Cl_x$ perovskites were both prepared by spin coating on top of substrate followed by a thermal annealing of 100℃ for 2 hours. The gold (Au) electrodes were thermally deposited with film thicknesses of 220 nm under the vacuum of 7×10^{-7} torr. The Seebeck measurements were performed based on Au/perovskite/Au lateral device structure by using an InstruNet Model 100 Input/Output System. The Seebeck measurements were performed under dark condition. The Seebeck coefficient is defined as $S = \frac{\Delta V}{\Delta T}$ (ΔV =voltage difference; ΔT =temperature difference).

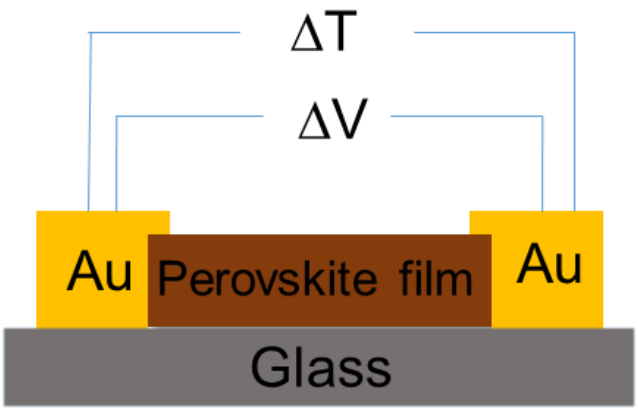

Figure 5.1 The device geometry for Seebeck measurements. ΔV: Seebeck voltage; ΔT: Temperature difference.

5.3 Results and Discussions

Figure 5.2(a) shows the Seebeck coefficients generated from the single organo-metal halide perovskite ($CH_3NH_3PbI_3$) and mixed organo-metal halide perovskite ($CH_3NH_3PbI_xCl_{3-x}$ with mole ratio of CH_3NH_3I: $PbCl_2$: PbI_2=1:0.3:0) under different temperatures. Here, the $CH_3NH_3PbI_3$ and $CH_3NH_3PbI_xCl_{3-x}$ organo-metal halide perovskites exhibit positive and negative Seebeck coefficients with large values of about 3.5 mV/K and -4.8mV/K at 80°C, respectively. This experimental result indicates that $CH_3NH_3PbI_3$ and $CH_3NH_3PbI_xCl_{3-x}$ organo-metal halide perovskites function as p-type and n-type semiconductors. Generally, the Seebeck effect is developed by charge diffusion driven by entropy difference between high and low temperature surfaces. The hole and electron diffusion can normally lead to positive and negative Seebeck effects under the driving force of entropy difference. Therefore, using the Seebeck coefficients can indicate the intrinsic property of charge transport (p-type or n-type) in organo-metal halide perovskites. Moreover, according to the large Seebeck coefficients and the electrical conductivities, 0.8*E-4 & 2.3*E-4 for single halide and mixed halide perovskite materials respectively based on the I-V curves by Keithley 2400, the power factors of the materials are calculated and shown in **Figure 5.2(b)**. We can see that the power factor of mixed halide perovskite is larger than that of single halide perovskite for thermoelectric application.

Now we confirm that the $CH_3NH_3PbI_3$ and $CH_3NH_3PbI_xCl_{3-x}$ (CH_3NH_3I: $PbCl_2$: PbI_2=1:0.3:0) perovskites are p-type and n-type semiconductors by using time-resolved photoluminescence with different types of quenching layer (as shown in **Figure 5.3**). Here we choose two different quenching layers: the poly(3,4-ethylenedioxythiophene) polystyrene sulfonate (PEDOT:PSS) and the Phenyl-C61-butyric acid methyl ester (PCBM). The PEDOT:PSS and PCBM are known as p-type and n-type materials. When a perovskite film forms a p-n type contact with PEDOT:PSS or PCBM, the photoluminescence from the perovskite film can be largely quenched.[185,186] Therefore, measuring photoluminescence quenching can provide an evidence to confirm the intrinsic n-type or p-type semiconducting properties in the $CH_3NH_3PbI_3$ and $CH_3NH_3PbI_xCl_{3-x}$ perovskite films. Figure 5.3(a) shows the results of the photoluminescence lifetime of $CH_3NH_3PbI_3$ perovskite with and without quenching

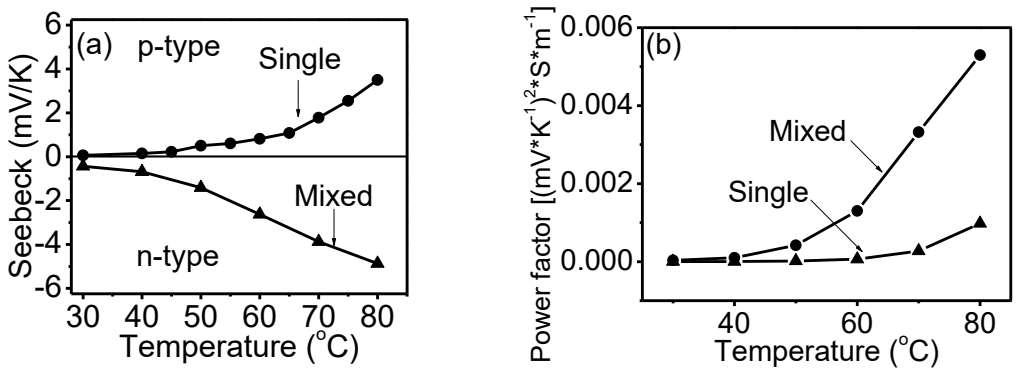

Figure 5.2 (a) The Seebeck effects & (b) power factor for organo-metal halide perovskite films based on lateral Au/perovskite/Au device design (●: $CH_3NH_3PbI_3$, ▲:$CH_3NH_3PbI_xCl_{3-x}$ with mole ratio of CH_3NH_3I: $PbCl_2$: PbI_2=1:0.3:0).

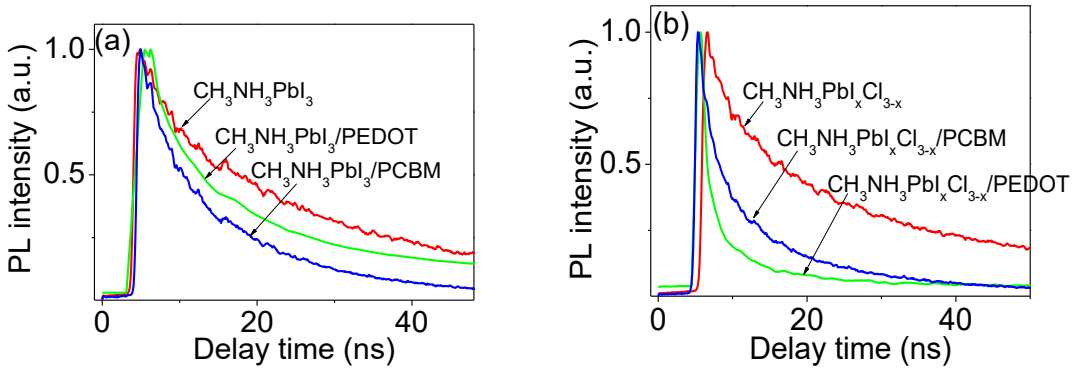

Figure 5.3 Time-resolved photoluminescence measurements from single-halide $CH_3NH_3PbI_3$ and mixed halide $CH_3NH_3PbI_xCl_{3-x}$ (mole ratio CH_3NH_3I: $PbCl_2$: PbI_2=1:0.3:0) with and without interfacial layers (PEDOT:PSS and PCBM). (a) Photoluminescence delay characteristics for $CH_3NH_3PbI_3$, $CH_3NH_3PbI_3$/PCBM, and $CH_3NH_3PbI_3$/PEDOT:PSS. (b) Photoluminescence delay characteristics for $CH_3NH_3PbI_xCl_{3-x}$, $CH_3NH_3PbI_xCl_{3-x}$/PCBM, and $CH_3NH_3PbI_xCl_{3-x}$/PEDOT:PSS.

layers. We can see that applying p-type PEDOT:PSS and n-type PCBM quenching layers lead to a longer and shorter lifetimes on the photoluminescence from the $CH_3NH_3PbI_3$ perovskite. The lifetimes associated with the p-type PEDOT:PSS and n-type PCBM quenching layers are about 18 ns and 14 ns. This confirms that the single halide $CH_3NH_3PbI_3$ perovskite is a p-type semiconductor. On contrast, the $CH_3NH_3PbI_xCl_{3-x}$ perovskite exhibits longer (12 ns) and shorter (8 ns) photoluminescence lifetimes when the n-type PCBM and p-type PEDOT quenching layers are separately applied (Figure 5.3(b)). This shows that the mixed halide $CH_3NH_3PbI_xCl_{3-x}$ perovskite is an n-type semiconductor.

Now, we explore the possibilities of tuning semiconducting properties between n-type and p-type by using Seebeck measurements. **Figure 5.4** shows the Seebeck coefficient gradually tunable between positive and negative values by changing the molar ratio between PbI_2, and $PbCl_2$ components under different temperatures. This experimental result indicates that $CH_3NH_3PbI_3$ and $CH_3NH_3PbI_xCl_{3-x}$ organo-metal halide perovskites function as p-type and n-type semiconductors. Changing the molar ratio between $PbCl_2$ and PbI_2 components allows the modification on the content volume of chloride ions in organo-metal halide perovskite crystals. It can be seen that the Seebeck coefficient changes from positive value to negative value when the concentration of chloride ions are increased. This means that increasing the chloride ions concentration can change the semiconducting properties from p-type to n-type by switching the majority carriers from holes to electrons. It is known that the presence of $CH_3NH_3^+$ vacancy can lead to p-type semiconducting properties[187,188] by downward shifting the Femi level. When the chloride ions are introduced in the organo-metal halide perovskites, on one hand, the $CH_3NH_3^+$ vacancies can be eliminated by removing the by-product of CH_3NH_3Cl during the formation of organo-metal halide perovskite polycrystals.[189] Obviously, as the $CH_3NH_3^+$ vacancies are eliminated, the chloride doped organo-metal halide perovskites can demonstrate n-type characteristics by upward-shifting the Fermi level. On the other hand, it has been found that positively charged vacancies, the iodine vacancies in the perovskite polycrystals can act as electron traps.[190] The vacancies originate from the distorted polycrystalline structures caused by impurities during the formation process of polycrystalline domains. It is also noted that the chloride ions can prevent the distortion of polycrystalline structures and increase the crystallinity by reducing the impurities in perovskite precursors and thus reduce the density of positively charged vacancies.[191-193] As a result, when the density

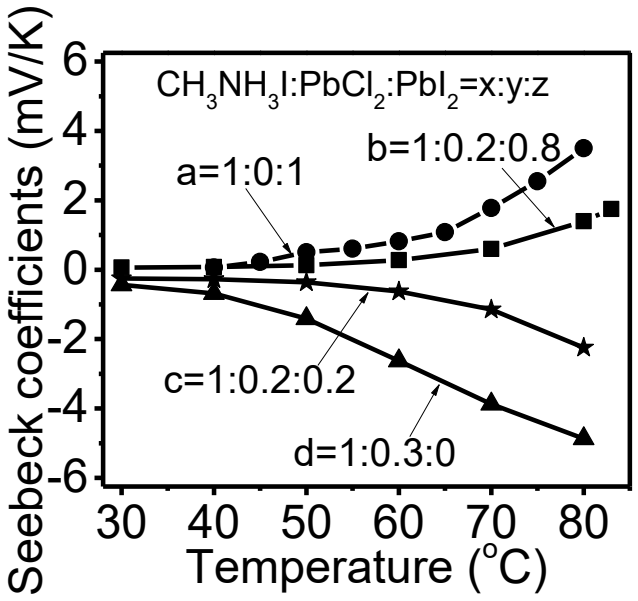

Figure 5.4 Seebeck effects from lateral perovskite devices with different component mole ratios. a: CH_3NH_3I: $PbCl_2$: PbI_2=1:0:1; b: CH_3NH_3I: $PbCl_2$: PbI_2=1:0.2:0.8; c: CH_3NH_3I: $PbCl_2$: PbI_2=1: 0.2:0.2; d: CH_3NH_3I: $PbCl_2$: PbI_2=1:0.3:0.

of electron trapping vacancies is gradually reduced by the introduction of chloride ions, the n-type characteristics will become more predominant in organo-metal halide perovskites. Therefore, the chloride ions can serve as the dopants to reduce the density of both $CH_3NH_3^+$ vacancies and electron trap sites from positively charged vacancies (+), which can increase the n-type characteristics in the chloride doped organo-metal halide perovskites.

We further note in Figure 5.4 that the magnitude of Seebeck coefficient is large and increases with increasing temperature within the given temperature range. This phenomenon suggests that the electrical polarization effect in the film can be accountable for the relatively large temperature-dependent Seebeck coefficients. Now, we use the capacitance-frequency (C-f) measurements to explore the temperature effects on local polarizations in bulk perovskite films. The capacitance-frequency (C-f) measurement were performed under dark condition by using dielectric spectrometer (Agilent E4980A LCR). In general, the capacitance-frequency characteristics can be divided into low and high-frequency regimes. The former and latter are associated with the electrode interface and bulk behaviors. **Figure 5.5** shows the frequency-dependent capacitance signals at different temperatures. At high frequency the capacitance signals can essentially reflect the bulk polarization in organo-metal halide perovskite films.[185] Here, we can see that at high frequency (> 100×10^3 Hz) the capacitance increases with increasing temperature in the ITO/$CH_3NH_3PbI_3$/Au device. This behavior indicates that increasing temperature can essentially lead to an increase in the bulk polarization in the single halide $CH_3NH_3PbI_3$ perovskite, functioning as p-type semiconductor. With increasing bulk polarization we can expect that the charge transport experiences less Coulomb scattering due to electrical screening effect, leading to an increase on carrier transport upon increasing temperature. The increase in the bulk polarization with increasing temperature can be due to the thermally activated detrapping process of electrons, which can lead to more positively charged trap sites in the p-type $CH_3NH_3PbI_3$ perovskite film with increasing temperature. This is because the trap states in perovskites have been demonstrated as shallow traps.[190] On contrast, we can see in Figure 5.5 that increasing temperature causes a decrease in the capacitance at high

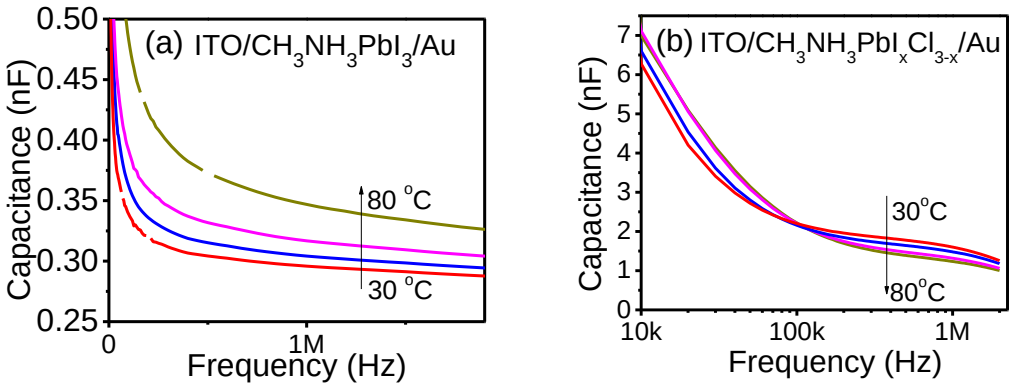

Figure 5.5 Capacitance-frequency (C-f) characteristics measured at different temperatures for ITO/Perovskite/Au devices. (a): Single halide $CH_3NH_3PbI_3$ perovskite, (b): Mixed halide $CH_3NH_3PbI_xCl_{3-x}$ perovskite (mole ratio CH_3NH_3I: $PbCl_2$: PbI_2=1:0.3:0). The C-f measurements were performed at 30, 60, 70, and 80°C.

frequency (>100×10^3 Hz) in the mixed halide perovskite based ITO/$CH_3NH_3PbI_xCl_{3-x}$(mole ratio CH_3NH_3I: $PbCl_2$: PbI_2=1:0.3:0)/Au device. This result implies that the bulk polarization decreases with increasing temperature in the mixed halide $CH_3NH_3PbI_xCl_{3-x}$ perovskite, functioning as n-type semiconductor. The decrease of bulk polarization upon increasing temperature can be due to the release of the trapped electrons, which can neutralize the positive defects in the n-type $CH_3NH_3PbI_xCl_{3-x}$ perovskite film with increasing temperature. In this situation, neutralizing the positive defects can decrease the Coulombic interactions to the majority carriers, namely electrons, and consequently enhances the electron transport upon increasing temperature. Therefore, the bulk polarization provides the underlying mechanism to influence carrier transport in both n-type and p-type organo-metal halide perovskites for development of Seebeck effect.

Figure 5.6(a) shows the XRD spectra of perovskite films. It can be seen that the peaks at 2θ=14º, 28 º, 32º reported in Figure 5.6(a), allowed us to identify the four thin films as the tetragonal perovskite structure.[194-196] In addition, for b, the peak at 2θ=12.5º indicates extra PbI_2 in the sample b film, which acts as defects in the perovskite film that can decrease the hole transport by scattering for the Seebeck development. **Figure 5.6(b)** shows absorption spectra of perovskite films, which also identify the thin films as perovskites.[197-199]

5.4 Conclusion

In this chapter, the Seebeck measurements were performed to study the n-type and p-type semiconducting properties in both single halide $CH_3NH_3PbI_3$ and mixed halide $CH_3NH_3PbI_xCl_{3-x}$ perovskites. We observed that the intrinsic semiconducting properties can be switched between n-type and p-type by changing the concentration of chloride ions during the formation of perovskite polycrystals. Here, we suggest that $CH_3NH_3^+$ vacancies and positively charged trap sites formed during crystallization process are the primary factor to determine the p-type semiconducting characteristic in the single halide $CH_3NH_3PbI_3$. On the other hand, introducing the chloride ions can decrease the density of $CH_3NH_3^+$ vacancies and positively charged trap sites during the formation process of

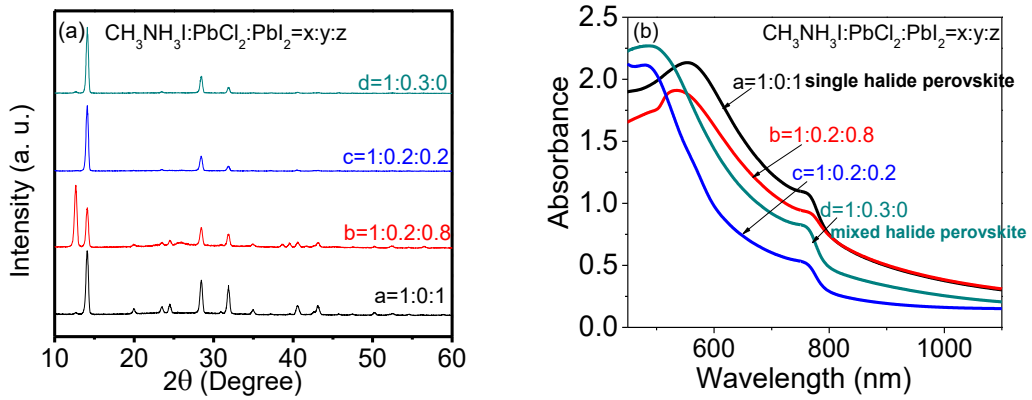

Figure 5.6 (a) XRD pattern (measured using Cu Kα radiation) and (b) absorption spectra of perovskite films with different initial mole ratio. a: CH_3NH_3I: $PbCl_2$: PbI_2=1:0:1; b: CH_3NH_3I: $PbCl_2$: PbI_2=1:0.2:0.8; c: CH_3NH_3I: $PbCl_2$: PbI_2=1: 0.2:0.2; d: CH_3NH_3I: $PbCl_2$: PbI_2=1:0.3:0.

organo-metal halide perovskites, leading to a n-type semiconducting properties in the mixed halide $CH_3NH_3PbI_xCl_{3-x}$ perovskites (mole ratio CH_3NH_3I: $PbCl_2$: PbI_2=1:0.3:0). Moreover, the large temperature-dependent Seebeck effects indicate that electrical polarization effect in the film can lead to an increase on carrier transport in the Seebeck development. Our capacitance-frequency measurements reveal that increasing temperature causes an increase and a decrease on bulk polarization in single and mixed halide perovskites, respectively. In the p-type single halide $CH_3NH_3PbI_3$ perovskite, increasing bulk polarization can decrease the Coulomb scattering to the majority carriers (holes), leading to an increase on hole transport for Seebeck development. In the mixed halide $CH_3NH_3PbI_xCl_{3-x}$ perovskite (mole ratio CH_3NH_3I: $PbCl_2$: PbI_2=1:0.3:0), decreasing bulk polarization can decrease the Coulomb interactions to the majority carriers (electrons), increasing electron transport for Seebeck development. Nevertheless, changing bulk polarization can present a convenient mechanism to influence carrier transport for Seebeck development. Clearly, our studies provide an insight on tuning intrinsic bulk polarization and semiconducting properties in organo-metal halide perovskites.

Chapter 6

6 Conclusions

Temperature-dependent surface polarization was explored as an additional driving force to diffuse charge carriers from low to high-temperature surface towards the development of high Seebeck effects based on vertical metal/polymer/metal thin-film devices. The research includes the following four parts.

First, a new mechanism was explored to develop Seebeck effects by using temperature-dependent surface polarization based on vertical multi-layer Al/P3HT:PCBM/Al thin-film devices. Here, the temperature-dependent surface polarization functions as an additional driving force, as compared with the traditional driving force from entropy difference, to diffuse the charge carriers under a temperature gradient towards the development of Seebeck effects. The temperature-dependent surface polarization is essentially generated by both the thermally dependent polarization through charge-phonon coupling mechanism and the thermally modulated interface dipoles by Fermi electrons. It is noted that the entropy difference often causes an inverse relationship between Seebeck coefficient and electrical conductivity in thermoelectric developments. However, this temperature-dependent surface polarization was found to provide a mechanism allowing a co-operative relationship between Seebeck coefficient and electrical conductivity. It was found simultaneously enhanced Seebeck coefficient and electrical conductivity by using dielectric interface through the temperature-dependent surface polarization to diffuse charge carriers in the Al/MoO_3/P3HT:PCBM/Al thin-film device.

Second, dual driving forces, namely surface-polarization difference and entropy difference, were found to co-develop Seebeck effects based on vertical multi-layer ITO/organic/Au devices. The organic materials include n-type PCBM (ground and excited states), PCBM:PMMA composites and n-type organic molecules [CN-MBE (1-cyano-1,2-bisbiphenyl-ethylene)]. It was found that both surface-polarization and entropy differences can drive mobile carriers between high and low-temperature

surfaces, leading to Seebeck effect. Essentially, the surface-polarization difference, caused by electron-phonon coupling on conductor/organic interface, establishes a temperature-dependent built-in field from high to low-temperature surface, drifting the negative carriers from low to high-temperature surface. This generates a positive Seebeck effect in the n-type conductor/organic/conductor devices. On contrast, the entropy difference still develops a negative Seebeck effect in n-type devices. The observed Seebeck effect reflects the contributions driven by both surface-polarization and entropy differences. It was also found that increasing electrical conductivity can tune the Seebeck effect from surface-polarization to entropy regime in all n-type ITO/PCBM/Au (ground and excited states), ITO/PCBM:PMMA/Au and ITO/CN-MBE/Au devices. The increased electrical conductivity in ITO/PCBM:PMMA/Au and ITO/CN-MBE/Au devices reflects the increase of charge mobility. Increasing charge mobility can decrease the interaction time between mobile charge and local polarization and consequently weakens the charge-phonon interaction. This essentially decreases the driving force from surface polarization in the development of Seebeck effect. Therefore, our studies presented a new mechanism to tune Seebeck effect by simultaneously using surface-polarization and entropy differences in the vertical multi-layer conductor/organic/conductor thin-film devices.

Third, Seebeck and cooling effects are two typical thermoelectric phenomena but with conflicting requirements on the relationship between electrical and thermal conductions. Here, we found the possibilities of using temperature-dependent surface polarization as a new thermoelectric driving force to solve this conflicting requirement in developing dual Seebeck and cooling effects based on the hybrid organic/inorganic Au/P(VDF-TrFE)/MoO_3/ITO thin-film device. On one hand, the temperature-dependent surface polarization can lead to a temperature-dependent electrical field between Au and ITO to drift charge carriers from high to low-temperature surface, generating Seebeck effect. On the other hand, the temperature-dependent surface polarization can absorb the heat from thermal vibration through charge-phonon coupling when the charge carriers are injected upon applying an electrical bias, leading

to a cooling effect. As a result, dual Seebeck and cooling effects are observed with large values (1.1 mV/K and 0.26 ºC) from the Au/P(VDF-TrFE)/MoO_3/ITO thin-film device. Therefore, it was found that the temperature-dependent surface polarization provides a mechanism to develop dual Seebeck and cooling effects through charge-phonon coupling based thin-film electrode/organic/electrode devices.

Fourth, Organo-metal halide perovskites can exhibit co-existed electrical polarizations and semiconducting properties respectively from organic and inorganic components. Here, we found that the Seebeck coefficient can be changed between positive and negative values when the concentration of chloride ions is varied between single-halide ($CH_3NH_3PbI_3$) and mixed-halide structures ($CH_3NH_3PbI_xCl_{3-x}$). This indicated that varying the concentration of chloride ions can tune the semiconducting properties between the n-type and p-type regimes in the organo-metal halide perovskites. Our temperature-dependent impedance measurement also showed that increasing temperature can cause a change on internal electrical polarization. As a result, we can propose that the internal polarization functions as the underlying mechanism responsible for large temperature-dependent Seebeck coefficients in organo-metal halide perovskites operating between n-type and p-type regimes.

In summary, our work can provide fundamental understanding for Seebeck development based on organic/inorganic hybrid structures. By combining the two driving forces, polarization and entropy difference, we can explore high Seebeck effect with controlled electrical conductivity; with tunable entropy and polarization regimes, we can control to explore semiconducting properties of the thin-film devices.

In the future work, we can consider about introducing high surface polarization effect into the thin-film device with high electrical conductivity to see what high surface polarization effect can do for the carriers in the devices with high electrical conductivity for Seebeck development.

References

1 C. B. Vining, *Nat. Mater.,* **2009**, *8* , 83

2 S. K. Yee, L. B. Saniya, E. G. Kenneth, D. Chris, *Energy Environ. Sci.,* **2013**, *6*, 2561 .

3 A. J. Minnich, M. S. Dresselhaus, Z. F. Ren, G. Chen, *Energy Environ. Sci.,* **2009**, *2*, 466-479.

4 M. Zebarjadi, K. Esfarjani, M. S. Dresselhaus, Z. F. Ren, G. Chen, *Energy Environ. Sci.,* **2012**, *5*, 5147.

5 J. P. Heremans, M. S. Dresselhaus, L. E. Bell, D. T. Morelli, *Nat. Nanotechnol.,* **2013**, *8*, 471.

6 Q. Zhang, Y. Sun, W. Xu, *D. Zhu, Adv. Mat.,* **2014**, *26,* 6829.

7 Z. D. Han, A. Fina, *Prog. Polym. Sci.* **2011**, *36*, 914.

8 O. Bubnova, Z. U. Khan, A. Malti, S. Braun, M. Fahlman, M. Berggren, X. Crispin, *Nat. Mater.,* **2011**, *10*, 429.

9 C. C. Liu, B. Y. Lu, J. Yan, J. K. Xu, R. R. Yue, Z. J. Zhu, S. Y. Zhou, X. J. Hu, Z. Zhang, P. Chen, *Synth. Met.,* **2010**, *160*, 2481.

10 A. J. Heeger, *J. Phys. Chem. B,* **2001**, *105*, 8475–8491.

11 A. G. MacDiarmid, *Angew. Chem., Int. Ed.,* **2001**, *40*, 2581–2590.

12 O. Bubnova, X. Crispin, *Energy & Environmental Science,* **2012,** *5*, 9345-9362.

13 L. Groenendaal, F. Jonas, D. Freitag, H. Pielartzik, J. R. Reynolds, *Adv. Mater.*, **2000**, *12*, 481–494.

14 K. Lee, S. Cho, S. Heum Park, A. J. Heeger, C.-W. Lee, S.-H. Lee, *Nature,* **2006**, *441*, 65–68.

15 X. Crispin, F. L. E. Jakobsson, A. Crispin, P. C. M. Grim, P. Andersson, A. Volodin, C. van Haesendonck, M. Van der Auweraer, W. R. Salaneck, M. Berggren, *Chem. Mater.,* **2006**, *18*, 4354–4360.

16 Ashizawa, S.; Horikawa, R.; Okuzaki, H. *Synth. Met*., **2005**, *153*, 5–8.

17 G. H. Kim , L. Shao , K. Zhang , K. P. Pipe, *Nat. Mater.,* **2013**, *12*, 719.

18 Y. M. Sun, P. Sheng, C. A. Di, F. Jiao, W. Xu, D. Qiu and D. B. Zhu, *Adv. Mater.,* **2012,** *24*, 932.

19 Q. Wei, M. Mukaida, K. Kirihara, Y. Naitoh, T. Ishida, *Materials,* **2015**, *8*, 732-750.

20 Z. Spitalsky, D. Tasis, K. Papagelis, C. Galiotis, *Prog. Polym. Sci.,* **2010**, *35*, 357.

21 C. Yu, Y. S. Kim, D. Kim, J. C. Grunlan, *Nano Lett.,* **2008**, *8*, 4428.

22 C. Yu, K. Choi, L. Yin, J. C. Grunlan, *ACS Nano*, **2011**, *5*, 7885.

23 C. Z. Meng, C. H. Liu, S. S. Fan, *Adv. Mater.*, **2010**, *22*, 535.

24 M. Scheele, N. Oeschler, K. Meier, A. Kornowski, C. Klinke, H. Weller, *Adv. Funct. Mater.*, **2009**, *19*, 476.

25 K. C. See, J. P. Feser, C. E. Chen, A. Majumdar, J. J. Urban, R. A. Segalman, *Nano Lett.*, **2010**, *10*, 4664.

26 M. He, J. Ge, Z. Q. Lin, X. H. Feng, X. W. Wang, H. B. Lu, Y. L. Yang, F. Qiu, *Energy Environ. Sci.*, **2012**, *5*, 8351.

27 M. Cutler, N. F. Mott, *Phys. Rev.*, **1969,** *181*, 1336.

28 J. P. Heremans, V. Jovovic, E. S. Toberer, A. Saramat, K. Kurosaki, A. Charoenphakdee, S. Yamanaka, G. J. Snyder, *Science*, **2008**, *321*, 554.

29 J. Sun, M. L.Yeh, B. J. Jung, B. Zhang, J. Feser, A. Majumdar, H. E. Katz, *Macromolecules*, **2010**, *43*, 2897.

30 B. Chandra, A. Afzali, N. Khare, M. M. El-Ashry, G. S. Tulevski, *Chem. Mater.*, **2010**, *22*, 5179.

31 I. Chung, J. H. Song, J. Im, J. Androulakis, C. D. Malliakas, H. Li, A. J. Freeman, J. T. Kenney, M. G. Kanatzidis, *J. Am. Chem. Soc.*, **2012**, *134*, 8579.

32 L. Yan, M. Shao, H. Wang, D. Dudis, A. Urbas, B. Hu, *Adv. Mater*. **2011**, *23*, 4120-4124.

33 S. Karpagam, S. Guhanathan, P. Sakthivel, *Polym. Bull.*, **2012**, *68*, 1023-1037.

34 H. Frohlick, *Theory Of Dielectrics*. Oxford University press, Oxford, 1956.

35 D. E. Yildiz,D. H. Apaydın, L. Toppare, A. Cirpan, *J. Appl. Polym. Sci.*, **2013**, *128*, 1659-1664.

36 S. Karpagam, S. Guhanathan, P. Sakthivel, *J. Appl. Polym. Sci.*, **2011,** *120*, 960-967.

37 L. Beverina, G. A. Pagani, *Acc. Chem. Res.*, **2014**, *47*, 319-329.

38 M. He, F. Qiu, Z. Lin, *Energy & Environmental Science*, **2013**, *6*, 1352-1361.

39 A. B. Kaiser, *Rep. Prog. Phys.*, **2001**, *64*, 1-49.

40 F. J. DiSalvo, *Science*, **1999**, *285*, 703-706.

41 R. Venkatasubramanian, E. Siivola, T. Colpitts, B. O'Quinn, *Nature*, **2001**, *413*, 597-602.

42 G. J. Snyder, E. S. Toberer, *Nat. Mater.*, **2008**, *7*, 105-114.

43 J. R. Sootsman, D. Y. Chung, M. G. Kanatzidis, *Angew. Chem. Int. Ed*,. **2009**, *48*, 8616-8639.

44 M. S. Dresselhaus, G. Chen, M. Y. Tang, R. Yang, H. Lee, D. Wang, Z. Ren, J.-P. Fleurial, P. Gogna, *Adv. Mater.,* **2007**, *19*, 1043-1053.

45 J. Yang, H.-L. Yip, A. K.-Y. Jen, *Adv. Energy Mater.*, **2013**, *3*, 549-565.

46 Y. W. Park , A. Denenstein, C. K. Chiang , A. J. Heeger, A. G. MacDiarmid, *Solid State Commun.,* **1979**, *29*, 747.

47 K. Kanamura,S. Yoshioka, Z. Takehara, *J. Electrochem. Soc.*, **1991**, *138*, 2165.

48 L. Yan, M. Shao, H. Wang, D. Dudis, A. Urbas, and B. Hu, *Adv. Mater.,* **2011**, *23*, 4120.

49 N. E. Coates, S. K. Yee, B. McCulloch, K. C. See, A. Majumdar, R. A. Segalman, J. J. Urban, *Adv. Mater.,* **2013**, *25*, 1629.

50 I. Jo, M. T. Pettes, J. Kim, K. Watanabe, T. Taniguchi, Z. Yao, L. Shi, *Nano Lett.,* **2013**, *13*, 550.

51 M. D. Losego, M. E. Grady, N. R. Sottos, D. G. Cahill, P. V. Braun, *Nat. Mater.,* **2012**, *11*, 502.

52 A. Pecchia, A. D. Carlo,A. Gagliardi, S. Sanna, T. Frauenheim, R. Gutierrez, *Nano Lett.,* **2004**, *4*, 2109.

53 Y. Yang, Z. Lin, T. Hou, F. Zhang, Z. Wang, *Nano Research,* **2012**, *5*, 888.

54 H. Song, C. Liu, H. Zhu, F. Kong, B. Lu, J. Xu, J. Wang, F. Zhao, *J. Electron. Mater.,* **2013**, *42*, 1268.

55 M. He, F. Qiu, Z. Lin, *Energy & Environmental Science,* **2013**, *6*, 1352.

56 A. Tan, J. Balachandran, S. Sadat, V. Gavini, B. D. Dunietz, S.-Y. Jang,P. Reddy, *J. Am. Chem. Soc.,* **2011**, *133*, 8838.

57 M. Paulsson, S. Datta, *Phys. Rev. B,* 2003, 67, 241403.

58 O. Bubnova, X. Crispin, *Energy & Environmental Science,* **2012**, *5*, 9345.

59 A. B. Kaiser, Rep. Prog. Phys., **2001**, *64*, 1.

60 E. L. Leguenza, R. L. Patyk, R. M. Q. Mello, L. Micaroni, M. Koehler,I. A. Hümmelgen, *J. Solid State Electrochem.,* **2006**, *11*, 577.

61 Y. Yuan, T. J. Reece, P. Sharma, S. Poddar, S. Ducharme, A. Gruverman, Y. Yang, J. Huang, *Nat. Mater.,* **2011**, *10*, 296.

62 H. -L. Yip, S. K. Hau, N. S. Baek, H. Ma, A. K. -Y. Jen, *Adv. Mater.***2008**, *20*, 2376.

63 M. Sayer, A. Mansingh, J. B. Webb, J. Noad, *J. Phys. C: Solid State Phys.*, **1978**, *11*, 315.

64 C. Bounioux, P. Díaz-Chao, M. Campoy-Quiles, M. S. Martín-González, A. R. Goñi, R. Yerushalmi-Rozen, C. Müller, *Energy &Environmental Science*, **2013**, *6*, 918.

65 J. C. Duda, P. E. Hopkins, Y. Shen, M. C. Gupta, *Appl. Phys. Lett.*, **2013**, *102*, 251912.

66 J. C. Duda, P. E. Hopkins, Y. Shen, M. C. Gupta, *Phys. Rev. Lett.*, **2013**, *110*, 015902.

67 J. Clark, C. Silva, R. Friend, F. Spano, *Phys. Rev. Lett.*, **2007**, *98*, 206406.

68 R. Hildner, U. Lemmer, U. Scherf, M. van Heel, J. Köhler, *Adv. Mater.*, **2007**, *19*, 1978.

69 E. G. Maksimov, G. P. Motulevich, *Soviet Physics Jetp*, **1972**, *34*, 219.

70 A. H. Castro Neto, F. Guinea, *Phys. Rev. B*, **2007**, *75*, 045404.

71 S. Karpagam, S. Guhanathan, P. Sakthivel, *Polym. Bull.*, **2012**, *68*, 1023.

72 H. Frohlick, *Theory Of Dielectrics*. Oxford University press, Oxford, 1956.

73 D. E. Yildiz,D. H. Apaydın, L. Toppare, A. Cirpan, *J. Appl. Polym. Sci.*, **2013**, *128*, 1659.

74 S. Karpagam, S. Guhanathan, P. Sakthivel, *J. Appl. Polym. Sci.*, **2011**, *120*, 960.

75 L. Beverina, G. A. Pagani, *Acc. Chem. Res.*, **2014**, *47*, 319.

76 P. Amsalem, J. Niederhausen, A. Wilke, G. Heimel, R. Schlesinger, S. Winkler, A. Vollmer, J. Rabe,N. Koch,*Phys. Rev. B*, **2013**, *87*, 035440.

77 Y. Yuan, T. J. Reece, P. Sharma, S. Poddar, S. Ducharme, A. Gruverman, Y. Yang, J. Huang, *Nat. Mater.*, **2011**, *10*, 296.

78 B. F. Heiniger, E. Bucher, J. Muller, *Phys. kondens. Materie*, **1966**, *5*, 243.

79 C. Yoon, M. Reghu, D. Moses, A. Heeger,Y. Cao, *Phys. Rev. B*, **1993**, *48*, 14080.

80 A. Kaiser, *Phys. Rev. B*, **1989**, *40*, 2806.

81 N.T. Kemp, A. B. Kaiser,C. Liu, B. Chapman, O. Mercier, A. M. Carr, H. J. Trodahl, R. G. Buckley, A. C. Partridge, J. Y. Lee, C. Y. Kim, A. Bartl, L. Dunsch, W. T. Smith, J. S. Shapiro, *J. Polym.Sci., Part B: Polym. Phys.*, **1999**, *37*, 953.

82 C. M. Jaworski, M. D. Nielsen, H. Wang, S. N. Girard, W. Cai, W. D. Porter, M. G. Kanatzidis,J. P. Heremans, *Phys. Rev. B*, **2013**, *87*, 045203.

83 W. Tian, R. Yang, *Appl. Phys. Lett.*, **2007**, *90*, 263105.

84 X. Huang, M. Roushan, T. J. Emge, W. Bi, S. Thiagarajan, J. H. Cheng, R. Yang, J. Li, *Angew. Chem. Int. Ed.*, **2009**, *48*, 7871.

85 V. Shrotriya, G. Li, Y. Yao, C. -W. Chu, Y. Yang, *Appl. Phys.Lett.*, **2006**, *88*, 073508.

86 Y. Nakayama, K. Morii, Y. Suzuki, H. Machida, S. Kera, N. Ueno, H. Kitagawa, Y. Noguchi, H. Ishii, *Adv. Funct. Mater.*, **2009**, *19*, 3746.

87 M. C. Gwinner, R. D. Pietro, Y. V., K. J. Greenberg, P. K. H. Ho, R. H. Friend, H. Sirringhaus, *Adv. Funct. Mater.*, **2011**, *21*, 1432.

88 J. Meyer, S. Hamwi, M. Kroger, W. Kowalsky, T. Riedl, A. Kahn, *Adv. Mater.*, **2012**, *24*, 5408.

89 C. P. Smyth, *Dielectric Behavior And Structure*, McGraw-Hill book company, New York, Toronto, London, 1955.

90 M. Akram, A. Javed, T. Z. Rizvi, *Turk J Phys*., **2005**, *29*, 355.

91 Lei He, M. Li, A. Urbas, B. Hu, *Adv. Mater.*, **2014**, *26*, 3956.

92 N. W. Cheung, S. K. Cheung, *Appl. Phys. Lett.*, **1986**, *49*, 85.

93 F. Yakuphanoglu, *J. Phys. Chem. Solids*, **2008**, *69*, 949.

94 Ş. Karataş,A. Türüt, *Physica B: Condensed Matter*, **2006**, *381*, 199.

80 J. Subbiah, D.Y. Kim, M. Hartel, F. So, *Appl. Phys. Let.*, **2010**, *96*, 063303.

96 J. Yang, Y. Xiao, Y. Deng, S. Duhm, N. Ueno, S. -T. Lee, Y. Li, J. Tang, *Adv. Funct. Mater.*, **2012**, *22*, 600.

97 D. Hu, Q. Liu, J. Tisdale, T. Lei, J. Pei, H. Wang, A. Urbas, B. Hu, *ACS Nano*, **2015**, *9*, 5208-5213.

98 Q. Liu, D. Hu, H. Wang, M. Stanford, H. Wang, B. Hu, *Phys. Chem. Chem. Phys.*, **2014**, *16*, 22201-22206.

99 D. Hu, Q. Liu, J. Tisdale, H. Nam, S. Park, H. Wang, A. Urbas, B. Hu, *Organic Electronics*, **2015**, *26*, 117-120.

100 S. Karpagam, S. Guhanathan, P. Sakthivel, *Polym. Bull.*, **2012**, *68*, 1023-1037.

101 H. Frohlick, *Theory Of Dielectrics*. Oxford University press, Oxford, 1956.

102 D. E. Yildiz, D. H. Apaydın, L. Toppare, A. Cirpan, *J. Appl. Polym. Sci.*, **2013**, *128*, 1659-1664.

103 S. Karpagam, S. Guhanathan, P. Sakthivel, *J. Appl. Polym. Sci.*, **2011**, *120*, 960-967.

104 L. Beverina, G. A. Pagani, *Acc. Chem. Res.*, **2014**, *47*, 319-329.

105 M. He, F. Qiu, Z. Lin, *Energy & Environmental Science*, **2013**, *6*, 1352-1361.

106 O. Bubnova, X. Crispin, *Energy & Environmental Science*, **2012**, *5*, 9345-9362.

107 A. B. Kaiser, *Rep. Prog. Phys.*, **2001**, *64*, 1-49.

108 J. P. Heremans, V. Jovovic, E. S. Toberer, A. Saramat, K. Kurosaki, A. Charoenphakdee, S. Yamanaka, G. J. Snyder, *Science*, **2008**, *321*, 554-557.

109 F. J. DiSalvo, *Science*, **1999**, *285*, 703-706.

110 M. Cutler, N. F. Mott, *Phys. Rev.*, **1969**, *181*, 1336.

111 O. Bubnova, Z. Khan, A. Malti, S. Braun, M. Fahlman, M. Berggren, X. Crispin, *Nat. Mater.*, **2011**, *10*, 429-433.

112 R. Venkatasubramanian, E. Siivola, T. Colpitts, B. O'Quinn, *Nature*, **2001**, *413*, 597-602.

113 G. J. Snyder, E. S. Toberer, *Nat. Mater.*, **2008**, *7*, 105-114.

114 G-H. Kim, L. Shao, K. Zhang, K. P. Pipe, *Nat. Mater.*, **2013**, *12*, 719-723.

115 J. R. Sootsman, D. Y. Chung, M. G. Kanatzidis, *Angew. Chem. Int. Ed.*, **2009**, *48*, 8616-8639.

116 M. S. Dresselhaus, G. Chen, M. Y. Tang, R. Yang, H. Lee, D. Wang, Z. Ren, J.-P. Fleurial, P. Gogna, *Adv. Mater.*, **2007**, *19*, 1043-1053.

117 J. Yang, H.-L. Yip, A. K.-Y. Jen, *Adv. Energy Mater.*, **2013**, *3*, 549-565.

118 H. Nam, M. Granier, B. Boury, S. Park, *Langmuir*, **2006**, *22*, 7132–7134

119 W. Huang, J, Peng, L. Wang, J. Wang, Y. Cao, *Appl. Phys. Lett.*, **2008**, *92*, 013308.

120 Q. Liu, T. Wu, Y. Hsiao, M. Li, D. Hu, H. Wang, H. Xu, J. Tisdale, B. Hu, *J. Mater. Chem. A*, **2015**, *3*, 14431-14437.

121 R. A. Street, K. W. Song, S. Cowan, *Org. Electron.*, **2011**, *12*, 244-248.

122 W.-L. Leong, S. Cowan, A. Heeger, *Adv. Energy Mater.*, **2011**, *1*, 517-522.

123 J. Xi, D. Wang, Y. Yi, Z. Shuai, *J. Chem. Phys.*, **2014**, *141*, 034704.

124 W. Chr. Germs, K. Guo, R. A. J. Janssen, M. Kemerink, *Phys. Rew. Lett.*, **2012**, *109*, 016601.

125 O. Bubnova, Z. Khan, H. Wang, S. Braun, D. Evans, M. Fabretto, P. Hojati-Talemi, D. Dagnelund, J. Arlin, Y. Geerts, S. Desbief, D. Breiby, J. Andreasen, R. Lazzaroni, W. Chen, I. Zozoulenko, M. Fahlman, P. Murphy, M. Berggren, X. Crispin, *Nat. Mater.*, **2014**, *13*, 190.

126 G-H. Kim, L. Shao, K. Zhang and K. P. Pipe, *Nat. Mater.* **2013**, *12*, 719.

127 N. E. Coates, S. K. Yee, B. McCulloch, K. C. See, A. Majumdar, R. A. Segalman, J. J. Urban, *Adv. Mater.*, **2013**, *25*, 1629.

128 C. Bounioux, P. Díaz-Chao, M. Campoy-Quiles, M. S. Martín-González, A. R. Goñi, R. Yerushalmi-Rozen, C. Müller, *Energy & Environmental Science*, **2013**, *6*, 918.

129 A. Shakouri, J. Bowers, *Appl. Phys. Lett.*, **1997**, *71*, 1234.

130 A. Shakouri, C. LaBounty, J. Piprek, P. Abraham, J. Bowers, *Appl. Phys. Lett.*, **1999**, *74*, 88.

131 A. Shakouri, C. LaBounty, J. Piprek, P. Abraham, J. Bowers, *Materials Research Society,* **1999**, *545*, 449.

132 O. Bubnova, X. Crispin, *Energy & Environmental Science,* **2012**, *5*, 9345.

133 T. O. Poehler, H. E. Katz, *Energy & Environmental Science,* **2012**, *5*, 8110.

134 M. He, F. Qiu, Z. Lin, *Energy & Environmental Science*, **2013**, *6*, 1352.

135 Q. Zhang, Y. Sun, W. Xu, D. Zhu, *Adv. Mater.,* **2014**, *DOI: 10.1002/adma.201305371*.

136 A. Shakouri, Y. L. Edwin, D. L. Smith, V. Narayanamurti, J. Bowers, *Microscale Thermophysical Engineering*, **1998**, *2*, 37-47.

137 A. Shakouri, J. Bowers, *Appl. Phys. Lett.*, **1997**, *71*, 1234-1236.

138 A. Shakouri, C. LaBounty, J. Piprek, P. Abraham, J. Bowers, *Appl. Phys. Lett.*, **1999**, *74*, 88.

139 A. Shakouri, C. LaBounty, J. Piprek, P. Abraham, J. Bowers, *Mat. Res. Soc. Symp. Proc.,* **1999**, *545*, 449-458.

140 Y. Nakayama, K. Morii, Y. Suzuki, H. Machida, S. Kera, N. Ueno, H. Kitagawa, Y. Noguchi, H. Ishii, *Adv. Funct. Mater.,* **2009**, *9*, 3746-3752.

141 M. C. Gwinner, R. D. Pietro, Y. Vaynzof, K. J. Greenberg, P. K. H. Ho, R. H. Friend, H. Sirringhaus, *Adv. Funct. Mater.,* **2011**, *21*, 1432-1441.

142 J. Subbiah, D. Y. Kim, M. Hartel, F. So, *Appl. Phys. Lett.*, **2010**, *96*, 063303.

143 V. Shrotriya, G. Li, Y. Yao, C. Chu, Y. Yang, *Appl. Phys. Lett.,* **2006**, *88*, 073508.

144 J. Yang, Y. Xiao, Y. Deng, S. Duhm, N. Ueno, S. Lee, Y. Li, J. Tang, *Adv. Funct. Mater.,* **2012**, *22*, 600-608.

145 M. Sayer, A. Mansingh, J. B. Webb, J. Noad, *J. Phys. C: Solid State Phys.,* **1978**, *11*, 315-329.

146 W. Huang, J, Peng, L. Wang, J. Wang, Y. Cao, *Appl. Phys. Lett.*, **2008**, *92*, 013308.

147 W. Leong, S. Cowan, A. Heeger, *Adv. Energy Mater.,* **2011**, *1*, 517-522.

148 R. A. Street , K. W. Song , S. Cowan , *Org. Electron.,* **2011**, *12*, 244-248.

149 J. Cao, X. Zhao, J. Zhao, J. Zha, G. Hu, Z. Dang, *ACS Appl. Mater. Inter.,* **2013**, *5*, 6915-6924.

150 Y. Li, X. Huang, Z. Hu, P. Jiang, S. Li, T. Tanaka, *ACS Appl. Mater. Inter.,* **2011**, *3*, 4396-4403.

151 M. Li, H. Wondergem, M. Spijkman, K. Asadi, I. Katsouras, P. W. M. Blom, D. M. de Leeuw, *Nat. Mater.,* **2013**, *12*, 433-488.

152 L. Cai, H. Qu, C. Lu, S. Ducharme, P. Dowben, J. Zhang, *Phys. Rev. B,* **200**4, *70*, 155411.

153 K. Matsushige, H. Yamada, H. Tanaka, T. Horiuchi, Chen, X. *Nanotechnology*, **1998**, *9*, 208- 211.

154 H. Qu, W. Yao, T. Garcia, J. Zhang, A. V. Sorokin, S. Ducharme, P. A. Dowben, V. M. Fridkin, *Appl. Phys. Lett.*, **2003**, *82*, 4322-4324.

155 Y. Yuan, T. J. Reece, P. Sharma, S. Poddar, S. Ducharme, A. Gruverman, Y. Yang, J. Huang, *Nat. Mater.,* **2011**, *10*, 296-302.

156 C. Duan, W. Mei, W.-G. Yin, J. Liu, J. Hardy, S. Ducharme, P. Dowben, *Phys. Rev. B,* **2004**, *69*, 235106.

157 J. Liu , S. Shao, G. Fang , B. Meng , Z. Xie, L. Wang, *Adv. Mater.*, **2012**, *24*, 2774-2779.

158 M. T. Greiner, L. Chai, M. G. Helander, W. Tang, Z. Lu, *Adv. Funct. Mater.,* **2012**, *22*, 4557.

159 A. J. Campbell, D. D. C. Bradley, J. Laubender, M. Sokolowski, *J. Appl. Phys.*, **1999**, *86*, 5004.

160 G. G. Malliaras, J. C. Scott, *J. Appl. Phys.*, **1999**, *85*, 7426.

161 A. M. Ionescu, H. Riel, *Nature*, **2011**, *479*, 329.

162 S. J. Martin, A. B. Walker, A. J. Campbell, D. D. C. Bradley, *J. Appl. Phys.*, **2005**, *98*, 063709.

163 S. A. DiBenedetto, A. Facchetti, M. A. Ratner, T. J. Marks, *Adv. Mater.,* **2009**, *21*, 1407.

164 M. Schidleja, C. Melzer, H. von Seggern, *Adv. Mater.,* **2009**, *21*, 1172.

165 P. Lara Bullejos, J. A. Jiménez Tejada, M. J. Deen, O. Marinov, W. R. Datars, *J. Appl. Phys.*, **2008**, *103*, 064504.

166 X. Qi, N. Li, S. R. Forrest, *J. Appl. Phys.* **2010**, *107*, 014514.

167 H. Zhou, Q. Chen, G. Li, S. Luo, T.-B. Song, H.-S. Duan, Z. Hing, J. You, Y. Liu, Y. Yang, *Science*, **2014**, *345*, 542-546.

168 J.-Y. Jeng, K.-C. Chen, T.-Y. Chiang, P.-Y. Lin, T.-D. Tsai, Y.-C. Chang, T.-F. Guo, P. Chen, T.-C. Wen, Y.-J. Hsu, *Adv. Mater*., **2014**, *26*, 4107-4113.

169 W. S. Yang, J. H. Noh, N. J. Jeon, Y. C. Kim, S. Ryu, J. Seo, S. I. Seok, *Science*, **2015**, *348*, 1234-1237.

170 Z. K. Tan, R. S. Moghaddam, M. L. Lai, P. Docampo, R. Higler, F. Deschler, M. Price, A. Sadhanala, L. M. Pazos, D. Credgington, F. Hanusch, T. Bein, H. J. Snaith, R. H. Friend, *Nat. Nanotechnol.*, **2014**, *9*, 687-692.

171 Y. H. Kim, H. Cho, J. H. Heo, T. S. Kim, N. Myoung, C. L. Lee, S. H. Im, T. W. Lee, *Adv. Mater.*, **2014**, *27*, 1248-1254.

172 J. Li, S. G. Bade, X. Shan, Z. Yu, *Adv. Mater.*, **2015**, *27*, 5196-5202.

173 G. Xing, N. Mathews, S. S. Lim, N. Yantara, X. Liu, D. Sabba, M. Gratzel, S. Mhaisalkar, T. C. Sum, *Nat. Mater.*, **2014**, *13*, 476-480.

174 H. Zhu, Y. Fu, F. Meng, X. Wu, Z. Gong, Q. Ding, M. V. Gustafsson, M. T. Trinh, S. Jin, X. Y. Zhu, *Nat. Mater.*, **2015**, *14*, 636-642.

175 Y.-C. Hsiao, T. Wu, M. Li, B. Hu,*Adv. Mater.*, **2015**, *27*, 2899-2906.

176 C. Zhang, D. Sun, C. X. Sheng, Y. X. Zhai, K. Mielczarek, A. Zakhidov, Z. V. Vardeny, *Nat Phys.*, **2015**, *11*, 427-434.

177 E. J. Juarez-Perez, R. S. Sanchez, L. Badia, G. Garcia-Belmonte, Y. S. Kang, I. Mora-Sero, J. Bisquert, *J. Phys. Chem. Lett.*, **2014**, *5*, 2390-2394.

178 J. M. Frost, K. T. Butler, F. Brivio, C. H. Hendon, M. van Schilfgaarde, A. Walsh, *Nanolett.*, **2014**, *14*, 2584-2590.

179 J. M. Frost, K. T. Butler, A. Walsh, *Apl Mater.*, **2014**, *2*, 081506.

180 G. Xing, N. Mathews, S. Sun, S. S. Lim, Y. M. Lam, M. Gratzel, S. Mhaisalkar and T. C. Sum, Science, **2013**, *342*, 344-347.

181 S. D. Stranks, G. E. Eperon, G. Grancini, C. Menelaou, M. J. P. Alcocer, T. Leijtens, L. M. Herz, A. Petrozza, H. J. Snaith, Science, 342 (2013), 341-344.

182 W. A. Laban and L. Etgar, *Energy Environ Sci.*, **2013**, *6*, 3249-3253.

183 M. M. Lee, J. Teuscher, T. Miyasaka, T. N. Murakami and H. J. Snaith, *Science*, **2012**, *338*, 643-647.

184 J. You, Z. Hong, Y. M. Yang, Q. Chen, M. Cai, T. B. Song, C. C. Chen, S. Lu, Y. Liu, H. Zhou and Y. Yang, *ACS nano*, **2014**, *8*, 1674-1680.

185 C. Zhao, B. Chen, X. Qiao, L. Luan, K. Lu, B. Hu, *Adv. Energy Mater.*, **2015**, *5*, 1500279.

186 P. Docampo, J. M. Ball, M. Darwich, G. E. Eperon, H. J. Snaith, *Nat. Commun.*, **2013**, *4*, 2761.

187 Z. Xiao, Y. Yuan, Y. Shao, Q. Wang, Q. Dong, C. Bi, P. Sharma, A. Gruverman, J. Huang, *Nat. Mater.*, **2015**, *14*, 193.

188 J. Kim, S. H. Lee, J. H. Lee, K. H. Hong, *J Phys Chem Lett*, **2014**, *5*, 1312.

189 H. Yu, F. Wang, F. Xie, W. Li, J. Chen, N. Zhao, *Adv. Funct. Mater.*, **2014**, *24*, 7102.

190 W. Yin, T. Shi, Y. Yan, *Adv. Mater.*, **2014**, *26*, 4653.

191 Q. Chen, H. Zhou, Y. Fang, A. Z. Stieg, T.-B. Song, H.-H. Wang, X. Xu, Y. Liu, S. Lu, J. You, P. Sun, J. McKay, M. S. Goorsky, Y. Yang, *Nat. Commun.*, **2015**, *6*, 7269.

192 Y. Tidhar, E. Edri, H. Weissman, D. Zohar, G. Hodes, D. Cahen, B. Rybtchinski, S. Kirmayer, *J. Am. Chem. Soc.*, **2014**, *136*, 13249-13256.

193 S. T. Williams, F. Zuo, C.-C. Chueh, C.-Y. Liao, P.-W. Liang, A. K. Y. Jen, *ACS Nano*, **2014**, *8*, 10640-10654.

194 M. Liu, M. Johnston, H. Snaith, *Nature*, **2013**, *000*, 1.

195 E. Unger, A. Bowring, C. Tassone, V. Pool, A. Gold-Parker, R. Cheacharoen, Kevin. Stone, E. Hoke, M. Toney, Michael D. McGehee, *Chem. Mater.*, **2014**, *26*, 7158-7165.

196 T. Song, Q. Chen, H. Zhou, C. Jiang, H. Wang, Y. (Michael) Yang, Y. Liu, J. You, Y. Yang, *J. Mater. Chem. A*, **2015**, *3*, 9032-9050.

197 J. Im, C. Lee, J. Lee, S. Park, N. Park, *Nanoscale*, **2011**, *3*, 4088-4093.

198 S. Colella, E. Mosconi, P. Fedeli, A. Listorti, F. Gazza, F. Orlandi, P. Ferro, T. Besagni, A. Rizzo, G. Calestani, G. Gigli, F. Angelis, R. Mosca, *Chem. Mater.*, **2013**, *25*, 4613-4618.

199 H. Kim, C. Lee, J. Im, K. Lee, T. Moehl, A. Marchioro, S. Moon, R. Humphry-Baker, J. Yum, J. Moser, M. Gra¨tzel, N. Park, *Scientific Reports*, **2012**, *2*, 591.

Vita

Qing Liu was born in Qixia, Yantai, Shandong Province, People's Republic of China. She received her B. S. in Polymer Chemistry and M. D. in Materials Science from Shanghai Jiaotong University in 2008 and 2011, respectively. Then she went to University of Tennessee, Knoxville, USA to pursue her PhD in the Department of Materials Science of Engineering under the supervision of Prof. Bin Hu starting from August, 2011.